LINKING MILLENNIAL SCALE VARIABILITY TO ORBITAL FREQUENCIES USING A HIGH RESOLUTION FORAMINIFERAL CLIMATE RECORD SPANNING THE PLEISTOCENE

by

Andre Scheinwald

A thesis submitted to the Faculty of the University of Delaware in partial fulfillment of the requirements for the degree Master of Science in Marine Studies

Spring 2013

LINKING MILLENNIAL SCALE VARIABILITY TO ORBITAL FREQUENCIES USING A HIGH RESOLUTION FORAMINIFERAL CLIMATE RECORD SPANNING THE PLEISTOCENE

by

Andre Scheinwald

Approved: ______________________________

Katharina Billups, Ph.D.
Professor in charge of thesis on behalf of the Advisory Committee

Approved: ______________________________

Mark A. Moline, Ph.D.
Director of the School of Marine Science and Policy

Approved: ______________________________

Nancy M. Targett, Ph.D.
Dean of the College of Earth, Ocean, and Environment

Approved: ______________________________

James G. Richards, Ph.D.
Vice Provost for Graduate and Professional Education

ACKNOWLEDGMENTS

I would like to thank everyone who has helped me throughout my time at CEOE. I am very thankful to my advisor Dr. Katharina Billups for giving me the opportunity to work with her and for all her patience, guidance, and assistance during my time here. I would also like to thank my committee members Dr. William J. Ullman and Dr. Dana E. Veron.

I am also grateful for my time with Dr. Paul Hall at Boston University and Dr. Randye Rutberg at CUNY Hunter College. They have both been a constant source of inspiration and aspiration. Their guidance and help throughout the years have helped lead me to where I am today.

My friends at CEOE have been an endless source of encouragement and companionship for the past two years. They kept me in good spirits and were always there when I needed them. I would also like to thank my childhood friends whom I grew up with. We've all come such a long way.

Special thanks go to my family for all their support- especially to my mom for her unconditional love and support, for tirelessly doing the thankless job, for always pushing me to do more, and for having faith in my abilities.

This material is based upon work supported by the National Science Foundation under Grant No. OCE-1060208. Furthermore, this research used samples provided by the Ocean Drilling Program (ODP). ODP is sponsored by the U.S. National Science Foundation (NSF) and participating countries under the management of the Joint Oceanographic Institutions, Inc.

TABLE OF CONTENTS

LIST OF TABLES

LIST OF FIGURES

ABSTRACT

I hypothesize that millennial-scale variability in the subtropical northwest Atlantic Ocean is a result of advective communication from the Equator of a non-linear response to orbital scale insolation forcing. To test the hypothesis, I have reconstructed sea surface hydrography in the northwestern subtropical Atlantic (31°40.461'N, 75°25.127'W) using a high resolution *Globigerinoides ruber senso lato* $\delta^{18}O$ record. The data from this study has been spliced with data from other regional publications to fill a gap in the $\delta^{18}O$ record from Marine Isotope Stages (MIS) 6 through 8 (129 Ka – 267 Ka) in order to reproduce a continuous, high resolution, $\delta^{18}O$ record spanning the Pleistocene. The spliced record allows for examination of high frequency, sub-orbital climate fluctuations throughout the Pleistocene. Work performed prior to this study determined that there is a shift in dominant precessional periodicities between 0-338 Ka (23 kyr) and 338-900 Ka (23 and 19 kyr). In order to determine whether changes in precession induces changes at the millennial scale, statistical analysis was performed on the spliced record using spectral power of two time periods from 0-338 Ka and 338-875 Ka. In the 0-338 Ka spectral analysis results indicated the presence of a half precessional signal at 12.5 kyr, close to the expected value of 11.5 kyr based on a 23 kyr periodicity. A higher frequency at 5.2 kyr was interpreted here to represent the quarter precession cycle (expected value of 5.8 kyr). Results from 338-875 Ka demonstrates two precessional peaks at 23.3 and 19.4 kyr

but are missing significant half precessional signals. Signals at 5.9 and 5.3 kyr are interpreted as the quarter precession cycle of the expected 23 kyr precessional signal with a resulting 5.8 kyr periodicity while the 4.9 and 4.4 kyr signals represent the quarter precession cycle of an expected 19 kyr signal with a resulting 4.8 kyr signal. However, multiple iterations of the age model determine that these results are not robust as the applied tuning method and age model used change the position and power of the peaks. Periodicities from ~1.5-4 kyr are resolvable at Site 1059 due to high sedimentation rates. This study shows that the timing of these peaks is age model independent and thus likely the results of processes occurring at higher frequencies such as heterodynes of centennial scale solar variations. Results demonstrate that changes in precessional timing and the resultant half and quarter precession signals may be related, but can only be resolved if the age model is precise.

Chapter 1

INTRODUCTION

The Pleistocene Epoch began at 2.6 Ma and ended at 11.7 Ka and is broken up into several unique events. There was the onset of Northern Hemisphere glaciation near the end of the Pliocene (2.7 Ma), the mid-Pleistocene transition (0.9 Ma), and the Mid-Brunhes Event at 0.4 Ma (Medina et al., 2008; Weirauch et al., 2008). Evidence from proxy records indicates that Northern Hemisphere glaciation began about 2.7 Ma (Shackleton et al., 1984; Ruddiman 2001). Prior to the mid-Pleistocene transition, climate signals indicate a 41 kyr trend which is commonly attributed to changes in the tilt of Earth's rotational axis with respect to its orbital axis around the Sun (obliquity). The 0.9 Ma mid Pleistocene transition marks the time when climate patterns shifted from a 41 kyr signal to a 100 kyr signal, with the amplitude of the 100 kyr signal increasing between 0.9 to 0.4 Ka. It is currently unknown what caused this shift, but there is evidence of maximum ice sheet extent and significant ice calving events preceding the evolution to the 100 kyr world (Mudelsee and Schulz, 1997). The Mid-Brunhes Event marks a time of high amplitude climate swings starting with a cool period during MIS 12 around 0.4 Ka. This was followed by a warm period during MIS 11, and a similar warm period at MIS 5e (Droxler and Farrell, 2000).

Millennial-scale oscillations (variations on the order of 1 kyr to 12 kyr) are present during the Pleistocene and lie superimposed over orbital-scale climate signals. Perturbations at the millennial-scale have been found in numerous studies at different sites using $\delta^{18}O$, Ice Rafted Debris (IRD), and ice cores. Several mechanisms have been suggested as the cause of millennial scale periodicities but no definitive theory explaining their origin has been determined (Hagelberg et al., 1994; McManus et al., 1999; Rutherford and D'Hondt, 2000; Billups et al., 2006; Jouzel et al., 2007; Weirauch et al., 2008; Margari et al., 2010).

The study of millennial-scale oscillations and what causes them also plays a role in the path and development of human history. The Holocene was a fairly stable climate which allowed for the establishment of civilization and the creation of successful trading hubs along coastlines. Development stalled during the Little Ice Age (LIA) which lasted from the 16th to 18th century. European crop practices during this period responded slowly to less reliable and shorter growing seasons, which led to famine from a decreased food supply (Reiter, 2000). Temperature shifted by 0.6°C during the LIA (Broecker, 2000), whereas during the Pleistocene, the fluctuations of millennial-scale oscillations have amplitudes that dwarf the LIA in comparison. It is necessary to have a complete record of $\delta^{18}O$ for the Pleistocene not only for its value for long-term statistical analysis, but also to determine the frequency of occurrence for these oscillations and determination of how likely rapid climate change may be today.

Here I investigate millennial-scale variations in surface water hydrography in the subtropical northwest Atlantic (Ocean Drilling Program Leg 172, Site 1059) from 129 Ka to 267 Ka filling a gap in an otherwise ~ 1 million year long millennial-scale record from this region. This site lies within the western boundary current of the Atlantic (Gulf Stream) and is a major source of heat to high latitudes, potentially affecting the behavior of Northern Hemisphere ice sheets. The site is located at 31°40.461'N, 75°25.127'W, on the Blake Outer Ridge, in the subtropical northwest Atlantic Ocean (Figure B.1)

I hypothesize that millennial-scale climate signals generated at Site 1059 are a non-linear response to orbital scale insolation forcing. The precessional signal (19 kyr and 23 kyr) results from two different properties known as precession of the ellipse and axial precession. When combined, the effect of these precessional motions affects the amount of insolation received by the Earth at different latitudes and different seasons (Figure B.2). A 10 and 12 ky signal cannot be attributed to Milankovitch scale oscillations because of the relatively short time-scale, which points to the possibility that the signal results from some non-linearity. Due to the quasi-cyclical nature of these planetary motions, non-linear responses to changes in precession are possible based on changes in insolation maxima. An analogy of this process occurs with the twice yearly passage of the sun over the equator during the equinox (Short et. al., 1991). This induces an equatorial climate response twice a year. Changes in Equatorial insolation induce changes in evaporation and precipitation which affects $\delta^{18}O$ values. The signal can be communicated to higher latitudes within a western boundary current which carries perturbed marine signals from the equatorial to northern Atlantic Ocean. It stands to reason that the half precessional signal will be detected at Site 1059 as it is located within the influence of the Gulf Stream; the North Atlantic western boundary current which transports warm waters from the tropics to higher latitudes.

I predict that quarter precession cycle signals will be detected at Site 1059 due to cross-latitudinal communication from the Gulf Stream. Quarter precessional cycles result from differences in insolation through time. Berger et al. (2006) modeled variations in insolation based on the summer and winter solstices as well as the spring and fall equinoxes. They found that taking the difference in maximum insolation of the equinoxes from minimum insolation of the solstices produced a signal with 5.5 kyr periodicity. This signal is identified as an equatorial quarter precession cycle which may be communicated from the Equator to higher latitudes via the Gulf Stream current.

In sum, this study seeks to test the hypothesis that millennial scale climate signals at Site 1059 are a product of a non-linear response to changes in precession by reconstructing a high resolution $\delta^{18}O$ record using planktonic foraminiferal species *Globigerinoides ruber*. This species serves as a proxy for sea surface hydrography, and will be used to analyze the hydrography of Site 1059 of the Ocean Drilling Program from 129 Ka to 267 Ka. Measurements of $\delta^{18}O$ values during MIS 6-8 (129-267 Ka) will cover a gap in time in the Pleistocene that has yet to be regionally studied in the subtropical northwest Atlantic. Combining this data with other publications will create a complete, continuous, high resolution reconstruction of $\delta^{18}O$ for the majority of the Pleistocene. Using spectral analysis this complete reconstruction will allow for detection of precessional variability and changes at half and quarter precession periodicities.

Chapter 2

BACKGROUND

2.1 Orbital Cycles

Earth's planetary motions within our Solar System are composed of variations in the tilt of Earth's rotational axis with respect to the orbital plane, wobble in the position of the rotational axis, and changes in spatial positioning and shape of Earth's revolution around the Sun. These variations are caused by interactions with gravitational forces between planetary bodies. These variations affect the relative position of Earth in space through time and induce changes in climate based on the evolving spatial relationship with the Sun. Milutin Milankovitch quantified these climatic changes through time by relating changes in insolation to three orbital components; eccentricity, obliquity, and precession (Milankovitch 1930).

Eccentricity is a measure of deviation from a circular shaped orbit of Earth around the Sun. It alters the distance between the Earth and Sun, and compared to the other orbital components, has minor strength in terms of insolation changes. Eccentricity has periodicities of about 100 kyr and about 400 kyr with the mathematical value fluctuating between 0 and 0.06 (Ruddiman, 2001).

Obliquity is the measure of the inclination of Earth's axis with respect to the planets' orbital plane. It modulates the intensity of seasons in both hemispheres through changes in tilt with variations between ~22º and 24º over a ~41 kyr period (Ruddiman, 2001). Seasonal variations based on changes in insolation are higher during periods of high obliquity that advance glacial extent. Conversely, during periods of low obliquity, seasonal variations are more muted and lead to glacial retreat.

Precession has two components: Axial precession and precession of the ellipse. Axial precession is described as the approximate circular rotation of Earth along its' central axis and its' relative position with respect to the sun. Precession of the ellipse describes changes in position of Earth's revolution around the sun (Figure B.2). Combined, precession has a periodicity of ~23 kyr with the effects most intensely felt at the Equator (Ruddiman, 2001). In the context of this study, it is notable that timing between precession minima (or maxima) has varied from ~17 to ~29 kyr due to gravitational interactions between planetary bodies in our solar system.

Spectral analysis of the insolation curve of the past 900 kyr (Lasker et al. 1993) shows that there is a change in dominant precessional periodictiy. From 0-340 Ka there is a strong 23 kyr periodicity, while from 340-900 Ka there are two precessional peaks at 23 and 19 kyr (Figure B.3). This data lends to the question of whether or not changes in the periodicity of precession between these two time periods affects changes in sub-orbital periodicities. If so, it would provide a link between millennial-scale and orbital-scale variations.

2.2 Millennial-Scale Variability

High sedimentation rate marine records have allowed for high resolution analysis of proxy records at the millennial scale. These cycles occur well below the Milankovitch band and are defined between periodicities of 1-12 kyr. Variability at these sub-orbital periodicities have been reproduced and documented for the Pleistocene in numerous climate records (Dansgaard et al., 1984; Chapman and Shackleton, 1998; Oppo et al., 1998; McManus et al., 1999; Billups et al., 2006). While Milankovitch-scale oscillations are better defined due to identification of the external forcing behind them (Hays et al., 1976); the same cannot be said about the millennial-scale, with several mechanisms having been suggested to explain variability at these sub-orbital bands.

Several dominant mechanisms have been proposed as the cause of millennial-scale oscillations. It has been suggested that periodicities ranging from 1 Ka to 12 Ka are climate signals induced by the harmonics of precession (Hagelberg et al., 1994; McManus et al., 1999; Weirauch et al., 2008) and is evident in $\delta^{18}O$ records from the Subtropical Northwest Atlantic (Billups et al., 2006; Weirauch et al., 2008). McManus et al., 1999 proposes that the extent of continental glaciation causes deflection of the Jet Stream which causes sea surface cooling at the millennial time-scale. Other possibilities include changes in deep ocean circulation (Jouzel et al., 2007; Margari et al., 2010), or increased heat flow in the surficial ocean, either laterally along the equator, or poleward to higher latitudes (Rutherford and D’Hondt, 2000).

The contribution of this study was the completion of a high resolution ~1.3 myr long record in the subtropical northwest Atlantic Ocean. A continuous high resolution record allows for analysis of millennial-scale oscillations and their potential cause. Determination of the frequency and amplitude of millennial scale oscillations are relevant to human development, as a stable climate has played a role in the path and development of our species. Our climate dependent development is evidenced through the Little Ice Age when an average decrease in temperatures of 0.6ºC resulted in famine due to changes in the growing season (Reiter, 2000; Broecker, 2000).

2.3 Site Location and Surface Hydrography

Site 1059 was cored on the Blake Outer Ridge (BOR) at a depth of 2996.7m, at 31°40.461'N, 75°25.127'W, in the subtropical northwest Atlantic Ocean (e.g., Figure B.1). Annual surface temperature for the region is ~25° with seasonal variations from approximately 22° averaged over January through March, to 28° from July to September (Figure B.4). In the winter the waters above Site 1059 are well mixed whereas there is greater stratification during the summer (Levitus et al. 1994, Figure B.4).

The site lies toward the northern boundary of the Gulf Stream (Figure B.1), a western boundary current, and is one of the primary mechanisms of heat transfer from tropical to sub-polar latitudes in the Atlantic Ocean (Broecker et al., 1985). Western boundary currents are generally fast moving and transport a significant volume of water (Garrison et al., 2002). Weaker transport induced by glacial climates results in a broader, slower, current which leads to a less defined boundary between slope waters and the western boundary current (Mann and Lazier, 1991).

It is reasonable to consider that changes in precessional periodicity and the resulting non-linear variations at the millennial-scale will be detected at Site 1059 as it lies within the relative boundaries of the Gulf Stream. Oppo et al., 2001 found 5-10 kyr surface variability at Site 1059 using *G. ruber* $\delta^{18}O$ during MIS 5. Other studies at this site have also found sub-orbital scale periodicities superimposed over the orbital scale signal from 1-3 kyr and 5-10 kyr using *G. ruber* $\delta^{18}O$ (Heusser et al., 2003; Healy and Thunell, 2004).

2.4 Sediments at Site 1059

Site 1059 lies within the Blake Outer Ridge sediment drift formation created by the Deep Western Boundary Current (Flood and Giosan, 2002) which carries a high sediment load eroded from the Canadian continental margin (Laine et al., 1994). This area is characterized by high sediment accumulation rates directly related to intermediate and deep-water circulation patterns, resulting in rapid deposition of terrigenous material and in-situ sediment (Yokokawa and Franz, 2002).

Three holes were drilled (Site 1059 A, B, C) and spliced together to form a composite in order to ensure complete stratigraphic recovery. Each progressive drill hole lies due southeast from the last with a total offset between the three sites amounting to 58m. All sections were taken with an Advanced Piston Corer with a recovery ranging from 91 to 109%. The high recovery percentage ensures that the sediment layers collected represent a continuous high resolution record with minimal gaps in time.

The lithology at Site 1059 alternates between clay rich and carbonate rich sediments intermittently interspersed by layers of red sediment (Keigwin et al., 1998). Composition of the sediments coincides with glacial vs. interglacial periods (Keigwin et al., 1998). During glacial intervals, there is a higher clay content which reflects increased terrigenous inputs, whereas during interglacial intervals there is a higher $CaCO_3$ content, indicating warmer periods (Gruetzner et. al., 2002). X-ray diffraction analysis of the site found a mineral composition of quartz, potassium feldspar, plagioclase, clay, calcite, dolomite, aragonite, pyrite, micas, and hematite. Grain size in the core is primarily clay and silt sized particles with clay color ranging from dark greenish gray to light brownish gray. Color Reflectivity of the core is related to carbonate content which seems to have cyclical variation (Keigwin et al., 1998). Low reflectivity coincides with low carbonate content and high reflectivity with high carbonate content. Overall, the site has high carbonate content with layers reaching up to 49 wt% with high test preservation due to a water depth which falls above the lysocline (Keigwin et al., 1998). Planktonic foraminiferal concentrations for this site are characterized as common to few.

2.5 Foraminiferal Species

Foraminifera are oceanic protozoans that are found as far back as the Cambrian in the geologic record (Prothero, 1998). They have a wide geographic range and are also found at different depth levels, from planktonic species to benthic. The tests are secreted from dissolved calcium and bicarbonate to create a calcareous shell. Abundance of specific foraminiferal species is dependent on local ocean temperature as well as depth in the water column. As they die, foraminifera fall down through the water column and settle out on the seafloor where they can be preserved in the sediment. Their abundance, geographic distribution, and sensitivity to local and global changes in temperature and chemistry, makes foraminifera a popular tool for paleo reconstructions.

This study utilizes *Globigerinoides ruber* which lives in the upper 50m of the water column (Wang, 2000; Lowenmark et al., 2005, Figure B.4). *G. ruber* is geographically restricted to tropical and temperate waters. It is present year round with a higher abundance in the summer (Hui-Ling, 2004). Analysis focuses on the white variety rather than the pink variety of *G. ruber* due to its higher and more consistent down-core abundance in the area. Within the white *G. ruber* species there are two morphotypes, senso stricto and senso lato (s.s and s.l., respectively, Wang 2000). Measurement of $\delta^{18}O$ values in this study only focuses on *G. ruber* senso lato because it is more consistently abundant down-core in this region (e.g., Billups et al., 2006, Weirauch et al., 2008).

In sum, *Globigerinoides ruber* is used at site 1059 because it is an ideal candidate for use in creating a $\delta^{18}O$ record for surface hydrography. It lives in the upper water column and records changes in $\delta^{18}O$ which reflect changes in sea surface temperature. It is abundant year round with a spring production bias, and is continuously abundant down-core. Vital effects induced by morphology are also well constrained.

2.6 Oxygen Isotopic Composition of Planktic Foraminifera

Foraminifera are widely used as a paleoceanographic climate tracer because of their ubiquity in the oceans and function as a recorder of oxygen isotope composition of seawater and temperature through changes in $\delta^{18}O$ values. Foraminiferal shells reflect the ratio of ^{18}O to ^{16}O through uptake of bicarbonate during the calcification process. This occurs via the chemical reaction:

$$Ca^{2+} + 2HCO_3^- \rightleftharpoons CaCO_3 + CO_2 + H_2O \qquad \text{eq. 1}$$

Through this process the calcified shells of foraminifera reflect the oxygen isotope ratio of seawater, with which bicarbonate equilibrates. In essence, then, the isotopic signature of foraminiferal shells reflects changes in ice volume and salinity, but as discussed below in section 2.6.3, also fluctuates as a function of local water temperature.

In measuring oxygen isotopes, it is not the direct ratio between ^{18}O and ^{16}O that is calculated, but is calculated as the per mil difference between the sample and a known standard value. Such standards that are used for oxygen isotopes are either the Standard Mean Ocean Water (SMOW) or Pee Dee Belemnite (PDB). This difference is derived through the equation:

$$\delta^{18}\mathrm{O} = \left(\frac{\frac{^{18}O}{^{16}O}(sample) - \frac{^{18}O}{^{16}O}(standard)}{\frac{^{18}O}{^{16}O}(standard)} \right) * 1000 \qquad \text{eq. 2}$$

2.6.1 Ice Volume effect on $\delta^{18}O$

Ice volume has the largest effect on fluctuations of oxygen isotope ratios. This occurs as a function of Rayleigh distillation towards high latitudes (Figure B.5). Changes in rates of evaporation and condensation change the concentration of oxygen isotopes in the seawater. The lighter ^{16}O isotope evaporates more readily due to a higher vibrational energy between the bonds in $H_2{}^{16}O$, which decreases the amount of energy necessary to break those bonds. This creates water vapor with a low isotope ratio. The ratios for condensate and vapor also decrease as latitude increases because the heavy ^{18}O isotope falls out of the vapor as precipitate due to the amount of energy necessary to keep it as a vapor. This causes the general bulk concentration of ^{18}O to decrease in relation to ^{16}O. The cross latitudinal transfer of water vapor induces a low $^{18}O/^{16}O$ ice sheet ratio. And as ice sheets grow, seawater becomes enriched in ^{18}O. Conversely, as they retreat, water becomes depleted in ^{18}O. This evolution of ice sheets through time impacts the isotopic signature of the seawater and the calcareous tests formed from it.

On longer time-scales ice volume has a strong effect on the $\delta^{18}O$ of seawater due to storage of $\delta^{18}O$ depleted water in the ice. However, changes in ice volume may not be a significant factor in $\delta^{18}O$ fluctuations of calcite at the millennial scale. With changes in ice volume occurring on 17 to 100, or 400 kyr timescales, its effect on fluctuations on $\delta^{18}O$ is assumed to be minimal for 10-12 kyr scale oscillations (Imbrie et al., 1984, Hyde et al., 2002). Sub-orbital scale climate forcing would occur at frequencies resulting in 1-12 kyr periodicities; with a response time of 100-10,000 years, ice volume effects on $\delta^{18}O$ fluctuations for the target periodicities of this study are minor (Ruddiman, 2001).

2.6.2 Evaporation and precipitation effects on $\delta^{18}O$

Salinity fluctuations occur linearly with $\delta^{18}O$ of seawater as a function of regional evaporation and precipitation (Fairbanks et. al., 1992). Increased evaporation increases salinity and increases the $^{18}O/^{16}O$ ratio, while increased precipitation decreases salinity and $^{18}O/^{16}O$. Although there are no known proxies to quantify salinity effects on $^{18}O/^{16}O$, as detailed below, I estimate that these variations are relatively small because of minor changes in salinity in the region as well as a shallow slope relationship between salinity and $\delta^{18}O$ of the seawater.

At Site 1059 salinity variation represents a minor component of $\delta^{18}O$ variability. Seasonally, salinity at Site 1059 changes by approximately 0.3 (Levitus, 1994) which can be seen in Figure B.6B. Fairbanks et. al. (1992) shows that the relationship between $\delta^{18}O$ and salinity in the Sargasso Sea and Gulf Stream is:

$$\delta^{18}O = 0.11(S) - 3.15 \qquad \text{eq. 3}$$

This equation shows that the $\delta^{18}O$ of seawater fluctuates seasonally from 0.03‰ at the surface to 0.008‰ at 50m depth (Figure B.6C). This was calculated by taking the seasonal fluctuations in salinity at depth, using the above equation, to find the $\delta^{18}O$ signal of seawater based only on salinity, and then finding the difference between the seasons. The largest $\delta^{18}O$ fluctuation of equilibrium calcite based on seasonal salinity and temperature fluctuations is ~1.48‰ at the surface (Figure B.6D). The seasonal $\delta^{18}O$ calcite signature based on salinity and temperature fluctuations was calculated using the derived values for $\delta^{18}O$ of seawater, measured seasonal temperature differences, and plugged into the Paleotemperature equation:

$$PT = 16.9\text{-}4.2(\delta^{18}O_c - \delta^{18}O_{sw}) + 0.13(\delta^{18}O_c - \delta^{18}O_{sw})^2 \qquad \text{eq. 4}$$

In order to solve this for $\delta^{18}O_c$ the equation is expressed linearly by dropping out + $0.13(\delta^{18}O_c - \delta^{18}O_{sw})^2$. The linear paleotemperature equation has been proven to be an adequate approximation for these calculations by Bemis et. al., 1998 with maximum seasonal temperature offsets of 0.9ºC.

As shown above, these seasonal variations in salinity are small and the $\delta^{18}O$ – salinity slope is low. Thus the effect of salinity on the $\delta^{18}O$ of calcite presents only a minor uncertainty. However, it does affect the absolute temperature calculation from $\delta^{18}O$ values. Therefore I interpret the $\delta^{18}O$ record largely in terms of hydrography.

2.6.3 Temperature effects

Local water temperature affects the ratio of ^{18}O to ^{16}O in biogenic calcite by changing the fractionation factor between $CaCO_3$ and H_2O. As water temperature increases, the fractionation factor decreases. This changes the degree of fractionation that occurs in the isotopic exchange between the calcite and water.

Chapter 3

APPROACH

The Grützner et al. (2002) age model was initially used to determine ages corresponding to the study interval for Site 1059 from a depth of 39.12 – 71.14 meters composite depth (mcd). Grützner et al. (2002) used the initial age model based on orbital tuning of variations in magnetic susceptibility from shipboard measurements. Initial spectral analyses of the shipboard measurements indicate significant power on orbital periods which validate the use of age control refinement based on astronomical tuning. Their age model was fine-tuned by utilizing estimated $CaCO_3$ measurements based on diffuse spectral reflectance records and precession (Grützner et al, 2002). 5 kyr was subtracted from the calculated ages to create a final age meant to compensate for phase lag between orbital forcing and the climate response.

Sedimentation rates have ranged from 13.7 to 40.9 cm/kyr during 129 Ka to 267 Ka based on the initial age model (Figure B.7). High sedimentation rates at Site 1059 coupled with a 5 cm sampling interval results in an average time step of 200 years. Anderson (2001) determined that at sedimentation rates of 25 cm/ky more than 80% of a millennial scale signal can be attributed to the original input and reaches up to 90% at 30 cm/ky. The high rate of sedimentation at the site, and its position above the lysocline, reduces the amount of dissolution of calcareous tests and attenuation of the climate signal from bioturbation, allowing for reconstruction of a high resolution climate record and the detection of millennial scale oscillations at Site 1059.

3.1 Record Splicing

Data from this study was spliced with other regional $\delta^{18}O$ records in order to reproduce a continuous high resolution record for the past 900 kyr (Figure B.8). These records are from (in temporal order) Hagen & Keigwin (2002), Heusser et al., (2003), this study, Billups et al., (2011), Billups et al., (2004), and Weirauch et al., (2008) (Table A.1). Billups et al. (2006), who measured both species, demonstrated that *G. ruber* has slightly higher amplitude variations than *G. sacculifer*, but the millennial-scale variations are similar. The minor offset between these two species makes corrections unnecessary. Wang (2000) determined that there is a 0.3‰ difference between *G. ruber* s.l. and s.s. Due to the use of mixed *G. ruber* samples in several studies, no corrections can be made for species effects between the two. Ultimately, correcting for species effects between the different studies is not crucial as this study is primarily concerned with the spacing between maxima and minima as opposed to interpreting their absolute amplitudes.

3.2 Insolation Tuning

The establishment of a preliminary age model based on Grützner et al. (2002) and the splicing of several regional records allowed for fine tuning of a continuous 900 kyr record based on insolation. The age model was developed by tuning the spliced $\delta^{18}O$ record to Northern Hemisphere (65ºN) summer insolation using the solution of Lasker et al. (2004) by visually matching prominent peaks and troughs between insolation and the $\delta^{18}O$ record using the software package Analyseries (Paillard, D., L. Labeyrie and P. Yiou, 1996). This tuning adjustment creates tie points between the records and interpolates between them by assuming linear sedimentation rates.

The tuned time series was then filtered with a 33 kyr high band pass filter in order to remove low frequency Milankovitch oscillations (Obliquity and Eccentricity). The resulting signal was then fine-tuned to precession. Accuracy was visually determined by matching maxima and minima in the filtered record to corresponding maxima and minima in the precession parameter of insolation with amplitude modulation also used as a determination factor.

3.2.1 Cross-spectral analysis

In order to further evaluate the tuning strategy, the $\delta^{18}O$ record was analyzed using cross-spectral analysis with insolation. Using the Arand software package, the $\delta^{18}O$ record was first interpolated to a constant 1 kyr time step in order to match the time step between insolation data points. The two records were then compared to determine their coherence and phase relationship. Crosspectral parameters were set to 500 lags for

865 values. The analysis was performed using a full linear detrend. Confidence level was set to 80% with a 2.67 x10^{-3} bandwidth. I expect a high coherence and in-phase relationship to support my tuning adjustments.

3.2.2 Spectral Analysis

Spectral analysis was performed in order to determine whether or not signals related to half and quarter precession cycles are present in the $\delta^{18}O$ record. The tuned $\delta^{18}O$ record was broken up into two time segments (0-338 kyr and 338-875 kyr) reflecting the time intervals characterized by 23 kyr precession forcing only and 23+19 kyr precession forcing. The 0-338 Ka record was analyzed using a 33 kyr high band pass filter with a 250 year timestep, while the 338-875 record was analyzed using a 33 kyr high band pass filter with a 450 year timestep. The time steps approximate the temporal resolution of the record based on sedimentation rates. High band pass filters are utilized in the spliced $\delta^{18}O$ record to remove orbital signals in order to better resolve higher frequencies. The filtered data was then analyzed for spectral power using the REDFIT38 software of Schulz and Mudelsee (2002).

3.3 Insolation retuning

The spliced $\delta^{18}O$ record based on the Grützner et al. (2002) age model was retuned to insolation in order to determine robustness of significant signals from the initial tuning. All previous methods of the initial insolation based tuning have been repeated but use more tie points between the insolation and $\delta^{18}O$ record at slightly different depths.

Cross-spectral and spectral analysis was performed on the $\delta^{18}O$ record following the same approach used for the initial insolation tuned record. The two time segments (0-338 and 338- 875) had average time steps of 249 years (250 years previously) and 796 years (450 years previously). The time steps approximate the temporal resolution of the record based on sedimentation rates and change based on minor differences in the age model. Cross-spectral parameters were set to 400 lags for 867 values. The analysis was performed using a full linear detrend. Confidence level was set to 80% with a 3.33 $x10^{-3}$ bandwidth.

3.4 Age Model Tuning to Lisiecki & Raymo (2005)

The initial spliced $\delta^{18}O$ record was tuned to Lisiecki & Raymo (2005, L&R 05) to provide additional control on the robustness of the interpretations. The L&R 05 benthic $\delta^{18}O$ stack derives from an average of 57 globally distributed benthic $\delta^{18}O$ records. The L&R 05 benthic stack was derived by automated graphic correlation between all the records to create a continuous splice. The record was then tuned to an ice volume model using the same automated method which results in a $\delta^{18}O$ signal that tracks obliquity. The spliced $\delta^{18}O$ record was conservatively tuned to the benthic stack using tie points between glacial and interglacial maxima and minima. Both the tuned record and the benthic stack were then filtered with a 33 kyr and 41 kyr high band pass filter for comparison of the precession and obliquity signals in both records.

3.4.1 Cross-Spectral Analysis

As outlined above, to determine tuning accuracy I compared the unfiltered $\delta^{18}O$ record tuned to L&R 05 to the L&R 05 benthic $\delta^{18}O$ stack using cross-spectral analysis. Both $\delta^{18}O$ records were assigned a 1 kyr time step using the Timer program within the Arand software suite in order to obtain a consistent Δt value between records. The records were then compared to determine correlation and phase based on 200 lags for 891 values. The analysis was performed with zero shift parameter and a full linear detrend. Confidence level was set to 80% with a 6.67 $x10^{-3}$ bandwidth.

3.4.2 L&R 05 Tuned Time Series Analysis

In order to determine whether or not millennial-scale periodicities are linked to specific age models, I also performed time series analysis on the $\delta^{18}O$ record tuned to L&R 05. Following the methods of time series analysis on the astronomically tuned age model, the record was broken into two time segments: 0-338 and 338- 875. The split records were filtered using a 33 kyr high-band pass filter at a 247 year time step (0-338 Ka) and a 779 year time step (338-875 Ka) with the resulting data analyzed for spectral power using the REDFIT38 software of Schulz and Mudelsee (2002).

Chapter 4

ANALYTICAL METHODS

Approximately 651 sediment samples with a volume of 10 cubic centimeters were obtained from ODP Site 1059 and analyzed using *G. ruber* s.l. to determine $\delta^{18}O$ values. Initial dry weight for all samples was attained before placement in a Na-hypochlorite/buffered DI solution bath for disaggregation. After disaggregation, the samples were rinsed with DI water through a 63μm sieve to remove the smaller size fraction. The remaining sample size was then dried and reweighed. The samples were then sieved to isolate the >212μm size fraction from which 7-15 *G. ruber* tests were picked per vial. All picked *ruber* tests were sonicated in DI water for eight seconds to remove any potential contamination from fine grained carbonate (e.g. coccoliths) stuck in the pores of the tests.

To measure $\delta^{18}O$ values, the tests were analyzed using an Elementar dual-inlet mass spectrometer equipped with a peripheral for the automated reaction of carbonate samples with phosphoric acid. The resulting $CO_{2(g)}$ from the acid-carbonate reaction were measured sequentially, ten times, against a standard reference gas calibrated to match the PeeDee Belemnite standard. The gases are ionized by a filament which acts as the ion source and passed through a magnetic field. Faraday cups calibrated to detect oxygen isotopes are used to determine $\delta^{18}O$ of the samples. Carrara Marble was used as an in-house standard positioned at the beginning and end of a run to correct for potential size or drift effects. Values were duplicated at targeted intervals to test the reproducibility of outlying data points and were averaged out when necessary. Random values (n=60) were also duplicated and averaged with the original data points.

Chapter 5

RESULTS

This study has bridged the previously unfilled gap between MIS 6-8 (Figure B.9A) in what was an otherwise continuous, high resolution, record spanning the Pleistocene (Figure B.9B). $\delta^{18}O$ maxima at 130-191 Ka and 243-300 Ka indicate glacial intervals of MIS 6 and MIS 8 (Figure B.9A). Conversely, $\delta^{18}O$ minima from 191-243 Ka coincide with interglacial MIS 7. Timing between MIS 6 and 8 is close to100 kyr which represent orbital scale variations in glacial extent.

The $\delta^{18}O$ record generated in this study is nearly continuous (Figure B.9A) Gaps in the record occur mainly during interglacial MIS 7 and are due to small sample size. These gaps range from 0.345 to 1.09 kyr. MIS 7 also has a lower sedimentation rate (Figure B.7) than the glacial intervals which accounts for the lower temporal resolution of the data points compared to the rest of the record (Figure B.9A).

High frequency $\delta^{18}O$ oscillations are superimposed over the Milankovitch scale fluctuations (Figure B.9A). Millennial-scale climate signals are more apparent in the younger portion of the $\delta^{18}O$ climate recordduring glacial MIS 6 (130-191 Ka) where fluctuations are visible by eye with multiple fluctuations in a 5 kyr time span.

The fluctuations still exist but are not as apparent during interglacial MIS 7 (Figure B.9A) with gaps in the record affecting high frequency resolution.

The $\delta^{18}O$ signal shifted during the Pleistocene from a dominant 41 kyr cycle to a 100 kyr cycle. The transition from a 41 kyr to 100 kyr cycle can be seen visually in the $\delta^{18}O$ signal by the increase in timing between glacial and interglacial climate after 900 Ka (Figure B.9B). The amplitude of the signal also increases after 900 Ka between glacial and interglacial climates, indicating a shift to more climate extremes. Extreme glacial periods occur during MIS 6, 8, 12, and 20 and are followed by rapid deglaciations. The older portion of the $\delta^{18}O$ record appears to have a lower sampling density but is related to a difference in time step between the various records.

5.1 Results from Initial Insolation tuning:

The spliced record from 0-900 Kyr was tuned to insolation by adjusting common features such as pronounced minima and maxima in the d18O record to corresponding features in the insolation record (Figure B.10). These adjustments create tie points between the records that are primary age control points. In this manner ages corresponding to the insolation curve can be transferred to the $\delta^{18}O$ record. Between the tie points, ages are derived by interpolation assuming an equal temporal spacing between data points (Figure B.10). The $\delta^{18}O$ record can be well matched to insolation by intervals of rapid $\delta^{18}O$ decrease corresponding to intervals of rapid insolation increase.

The precession component of the $\delta^{18}O$ record was compared to the precession component of insolation to select the most appropriate tie points (Figure B.11A). The filtered record can be matched well with the precessional signal (Figure B.11B). For example, the amplitude and periodicity of the adjusted record fits well with the precession component of insolation from 200 to 700 Ka. Each precessional cycle matches, as well as changes in the amplitude, the amplitude modulation. There is only one interval when the fit is not as good, at around 750 Ka. Here the $\delta^{18}O$ fluctuations are large while the precessional variations are small (Figure B.11B). An interval of high amplitude $\delta^{18}O$ fluctuations is apparent in the original time series from 750 to 800 Ka (Figure B.11A), and it may be that processes other than precession (e.g., obliquity) dominate the variations during that time period.

Cross spectral analysis of the insolation-tuned $\delta^{18}O$ record establishes the degree of correlation between the insolation record and the $\delta^{18}O$ record (Figure B.12A). Both records contain power at the main orbital periodicities of obliquity (41 kyr) and precession (23 and 19 kyr) and they are highly coherent ($k>0.9$, Figure B.12B). The records are out of phase with the tuned $\delta^{18}O$ record leading insolation by 18 degrees (2100 years) at the obliquity cycle (41 kyr) and by 8.1 degrees (428 years) at the 19 kyr signal (Figure B.12C). The records are in phase at the 23 kyr signal.

Spectral analysis from 0-338 Ka shows power at different frequencies. From 0-338 Ka, the $\delta^{18}O$ signal has significant precessional power (>95% confidence) occurring at 23.1 kyr periodicity. A 12.5 kyr peak contains significant spectral power above the 90% CI (Figure B.13). This signal possibly represents the 23 kyr half precession cycle as the expected value falls at 11.5 kyr. For a 23 kyr precession peak the quarter precession would occur at 5.8 kyr. A 19 kyr precession peak would have a corresponding signal of the quarter precession at 4.8 kyr. Spectral analysis for the 0-338 Ka time period has a 5.2 kyr signal above the 90% CI. A 19 kyr precessional signal is not present in the 0-338 Ka analysis, but there are peaks at 5.2 kyr and 4.8 kyr which are at the right periodicity for the quarter precession of the missing 19 kyr signal (Figure B.13). The average time step between data points from 0-338 kyr based on the insolation tuned age model allows for consideration of millennial scale oscillations at frequencies higher than quarter precession. Spectral analysis displays signals above the 95% CI at 3.26, 1.58, 1.44, 1.13, and 1.06 kyr. However, the 1.13 and 1.06 kyr signal are only four data points per cycle which is twice the Nyquist frequency for this data set and may be an artifact due to aliasing of the time series (Figure B.13).

Spectral analysis from 338-875 Ka reveals significant peaks at different frequencies. Significant precessional peaks occur at 23.3 and 19.4 kyr above the 95% CI (Figure B.14). The presence of an additional 19 kyr peak during the older time interval is consistent with the presence of this shorter precessional peak in the insolation record of this same time interval (Figure B.3). Based on the expected precessional signals at 23 and 19 kyr for 338-875 kyr the calculated half precessional peaks should respectively occur at 11.5 and 9.5 kyr. However, all potential half precessional signals fall well below the 90% CI which determines that it does not have enough strength to be significant (Figure B.14). Quarter precession signals are expected for a 23 and 19 kyr peak. Two values of significant power occur at 5.9 kyr above the 90% CI and 5.3 and 4.9 kyr above the 95% CI (Figure B.14). The 5.9 kyr signal falls within bandwidth of the calculated quarter precession for the peak 23 kyr signal. Both the 5.3 and 4.9 kyr peaks fall within bandwidth of the expected 19 kyr harmonic signal. Unlike spectral analysis of the 0-338 kyr section, the older time splice only goes back to a frequency of 0.3. This is due to the difference in average time step between the two records. With an average time step of 450 years, spectral analysis of the older section is cut off at a frequency of 0.3 kyr^{-1} in order to avoid approaching the Nyquist frequency.

5.2 Revised Insolation Tuning

Results from the initial insolation tuning were checked for age model effects by using new tie points between the unturned $\delta^{18}O$ record and insolation (Figure B.15). The new tie points still connect the most prominent $\delta^{18}O$ and insolation maxima and minima, but their position differs slightly in the choice of particular data points. Previous methods for tie point assignment from the initial insolation tuning were repeated for the revised tuning.

Again, it is possible to achieve an excellent overall fit between the precessional components of the $\delta^{18}O$ record and the insolation curve (Figure B.16B). The amplitude of the adjusted record fits particularly well with the precession component of insolation from 350 to 500 Ka. Two time periods where the periodicity of the tuned record does not quite match with precession occur at approximately 150 Ka and 650 Ka. And, there is a mismatch in amplitude from 750 to 800 Ka where it is apparent that the $\delta^{18}O$ fluctuations are larger than precession.

Cross spectral analysis of the retuned insolation based age model demonstrates the degree of correlation between the records (Figure B.17A, B). Both records have highly coherent (k>0.9) power at the Milankovitch scale periodicities of obliquity (41 kyr) and precession (23 and 19 kyr). The records are out of phase with the tuned record leading insolation by 20 degrees (2300 years) at the obliquity cycle (41 kyr), and 5 degrees (319 years) and 7 degrees (369 years) at both the 23 and 19 kyr signals (Figure B.17C).

For spectral analysis, the retuned $\delta^{18}O$ record was again split into two time slices (0-338 kyr and 338-875 kyr) (Figure B.18 and B.19). As in the previous age model, in the younger time slice there is a strong 23 kyr precessional signal (above 95%). But in this version, there is no power to indicate presence of half or quarter precession signals. A strong peak is present at 8.4 kyr (above 95%) that almost matches the power of the precessional peak. At the sub 5 kyr scale there are multiple significant peaks (> 95%) that may represent the same signal and have an average periodicity of 1.6 kyr (Figure B.18).

Spectral analysis of the second iteration of the insolation tuned age model from 338-875 kyr demonstrates significant peaks at different frequencies. Two precessional peaks occur at 22.9 and 19.1 kyr (above 90% and 95%, respectively). As in the previous age model, there is no power at half precession, but there are two peaks that occur at 5.9 and 5.1 kyr (Figure B.19). The 5.9 kyr peak may represent quarter precession of the 22.9 kyr precessional peak and the 5.1 kyr peak related to quarter precession of the 19.1 kyr signal (Figure B.19). Thus the presence of the higher frequencies related to the two precession peaks seems to be a robust feature consistent in both older section age models.

5.3 L&R tuning

Fine tuning of the insolation based age model illuminated a problem that minor tie point adjustments resulted in inconsistencies in the apparent significant periodicities at half and quarter precession which indicates a problem in the reproducibility of the millennial scale peaks. This is particularly true for the younger time interval. To determine to what degree millennial-scale periodicities are age model dependent, the initial, $\delta^{18}O$ record (on the age model reported by Grützner et al., 2002) was tuned to the Lisiecki and Raymo (2005) benthic $\delta^{18}O$ stack (L&R 05) which derives from an average of 57 globally distributed benthic $\delta^{18}O$ records. The continuous L&R 05 benthic $\delta^{18}O$ stack was derived by automated graphic correlation between the 57 global records which was then tuned to an ice volume model using the same automated method.

Tie points were assigned by matching the most pronounced maxima and minima between the spliced $\delta^{18}O$ record and L&R05 $\delta^{18}O$ stack (Figure B.20). Maxima and minima between the two records fit very well. However, finding matches between peaks of two records are difficult to determine on the finer scale (e.g., 750 Ka).

Correlation between the obliquity filtered $\delta^{18}O$ and L&R 05 record is high (Figure B.21A, B). Overall, the amplitudes of both filtered records are similar but are out of phase except for 100 to 200 Ka where the records match. The fit between the periodicity of the filtered $\delta^{18}O$ record and the precession filtered L&R record is generally poor (Figure B.21C). The amplitude of the tuned and adjusted record is consistently higher than the precession component of the L&R 05 record. This is most likely a result of smoothing of the L&R 05 record due to the average combined strength of the benthic foraminiferal $\delta^{18}O$ stack which reflect high latitude conditions and not precession, which is stronger at low latitudes. One section where the periodicity of the precession filtered record matches well with the precession filtered L&R 05 record at approximately 175 Ka to 250 Ka.

Cross-spectral analysis of the L&R 05 tuned $\delta^{18}O$ record demonstrates the coherency and phase between the two records (Figure B.22). Both records are highly coherent at the 41 kyr periodicity (k>0.9) and the 23 and 19 kyr periodicities (k>0.9, k>0.8, respectively (Figure B.22B)). The records are out of phase at the obliquity cycle with the tuned record leading the benthic record by 7 degrees (797 years). They are also out of phase with the tuned record lagging the benthic record by -9 and -27 degrees (575 and 1400 years, respectively) at both the 23 and 19 kyr signals (Figure B.22C).

Separating the $\delta^{18}O$ record into the two time intervals shows a different response from the previous two age models (Figure B.23 and B.24). From 0-338 Ka the precessional component of the $\delta^{18}O$ signal occurs at a 23.1 kyr periodicity above 95% confidence (Figure B.23). The half precession signal occurs at 11.6 kyr and is only significant above an 80% CI while no quarter precession signals are apparent (Figure B.23). The average time step from 0-338 kyr based on the L&R 05 tuned age model resembles that of the insolation tuned age model (~247 years) which allows for discussion of frequencies higher than quarter precession. Periodicities occur above either the 90% or 95% at 3.1, 2.8, 2.2, 1.8, 1.5, and 1.2 kyr. It is notable that the 1.5 kyr periodicity is consistent between age models even though periodicities at the half and quarter harmonic are not (Figure B.23).

Significant peaks occur in the 338-900 kyr time slice tuned to the L&R 05 age model. Precessional peaks occur at 23.3 and 18.1 kyr. The 23.3 kyr peak is only significant above an 80% CI while the 18.1 kyr peak is above 95% CI. A weak periodicity of 14.3 kyr is present above 90% CI (Figure B.24). This signal falls well outside the acceptable bandwidth of the expected half precession signal based on a 23 kyr precessional peak. Significant concentration of power occurs at 6.3, 4.7, 4.5 and 4.2 kyr (>90%). The 6.3 kyr signal does not correspond to the quarter precession of either precessional peak. The 4.7, 4.5, and 4.2 kyr signals are within bandwidth of the expected quarter precession cycle based on the 18.1 kyr precessional peak (Figure B.24). A quarter precession peak related to the 23 kyr precessional periodicity no longer occurs as it did in the other age models.

Results reveal that the expected half and quarter precession cycles vary in position and power between age models. The most consistent periodicities occurred at frequencies corresponding to precession and 1.5 kyr. The presence of both quarter precession periodicities in the older time interval where both primary precession periodicities are present is consistent between the two insolation tuned age models. The variations in half and quarter precession implies, particularly during the younger interval, that these signals may be too sensitive to and highly dependent on age model tuning. The robust 1.5 kyr signal points to processes that are not so sensitive to the choice of a particular age model.

Chapter 6

DISCUSSION

The high sedimentation at Site 1059 allows for detection of millennial scale high frequency signals superimposed in the climate record. Climate records of $\delta^{18}O$ during the Pleistocene from this site and others have documented millennial-scale variability ranging from 4-12 ky (Bond et al., 1993; McManus et al., 1999; Rutherford and D'Hondt, 2000; Billups et al., 2006; Billups et al., 2011). These high frequency signals are difficult to resolve when the $\delta^{18}O$ record is tuned to insolation because orbital scale periods drown them out in spectral analysis. However, high frequency signals become apparent in the subtropical northwest Atlantic regional record when high-pass filtering is used.

6.1 Half and Quarter Precession

Various mechanisms have been suggested as being responsible for high-amplitude millennial-scale oscillations. Van Geel et al. (1999) proposed that solar forcing is the cause of the variability by comparing changes in ^{10}Be to $\delta^{18}O$ from GISP2. Based on the matching age model for these records, solar forcing as the sole contributor seems unlikely, as the changes in ^{10}Be and $\delta^{18}O$ suggests an instantaneous response between solar variation and ice volume. Others hypothesize that high frequency variability is produced by harmonics and constructive interference from orbital-scale variability (Pestiaux et al., 1988; Steenbronk et al., 2003).

During the Pleistocene, several processes for millennial-scale oscillations have been put forth specifically at 10-12 kyr periodicities (half-precessional signal). Hagelberg et al. (1994) analyzed data from the eastern equatorial Pacific and Atlantic with a strong 10-12 kyr signal. The study hypothesized that the half-precessional signal represents a harmonic of precession. Cross-bispectral analyses highlighted nonlinear phase-coupling between the 10-12 kyr oscillations and precession ranging from 40% to 75%. They found that the signal may be related to a response in tropical precipitation and temperature changes induced by changes in maximum summer insolation, which is then transmitted to higher latitudes by advective transport. This suggested relationship corroborates the modeled findings of Short et al. (1991), which predicted a 10-12 kyr nonlinear signal based on changes in the suns position during perihelion and aphelion.

Rutherford and D'Hondt (2000) proposed two similar methods of generating a half-precessional signal transported up latitude by advective processes. The first method is by alignment of perihelion with each equinox during a single precession cycle with the resulting signal migrating to higher latitudes by advection (Short et al., 1991). Second, with the Northern and Southern hemisphere 180º out of phase with respect to precession, transport of the Southern hemisphere precessional signal to Northern latitudes induces a second northern insolation maximum.

Using cross-bispectral analyses of $\delta^{18}O$ against $CaCO_3$ accumulation, dust flux records, and Equatorial summer insolation values, Wara et al. (2000) found no significant relationship connecting nonlinearities to insolation forcing as did Hagelberg et al., (1994). This may be due to a difference in the types of records used, as Hagelberg et al., (1994) utilized records such as grayscale and %carbonate and Wara et al. (2000) used $\delta^{18}O$ values. While no relationship between equatorial insolation and half precession was found, there was coupling between changes in suborbital and lower-frequency variance, indicating a nonlinear ice/ocean/atmosphere response to orbital scale climate change (Wara et al., 2000). However, Ferretti et al. (2010) found a 10.7 kyr signal that was related to equatorial insolation with the response advecting to higher latitudes to their site in the North Atlantic. The incongruous results between Wara et al. (2000) and Ferretti et al. (2010) are interesting due to the study site locations. One of the site locations from Wara et al. (2000) was DSDP site 607 while Ferretti et al. (2010) looked at IODP site U1313, both of which have matching latitude and longitude.

Along with Wara et al. (2000), Billups et al. (2006) and McManus et al. (1999) both suggest that millennial-scale oscillations are modulated in terms of their amplitude by the extent of continental glaciation. This occurs through the deflection of the northern westerlies to lower latitudes, which causes cooling in surface water conditions. Billups et al. (2006) explain that the modern analogue of how this occurs is during winter months where winds are at their strongest and sea surface temperatures at their lowest. Hence the same conditions might apply to glacial periods. Numerical simulation models of the Last Glacial Maximum (LGM) determined that the jet stream and the westerlies were stronger and displaced to the south by ice sheets (Kutzbach and Guetter, 1986; Kutzbach et al., 1998).

5 kyr variability is evident in spectral analysis of the insolation tuned regional $\delta^{18}O$ record. From 0-338 kyr the signal is present at a 5.2 kyr periodicity. In the spectral analysis from 338-875 kyr there are several periodicities that occur at 5.9, 5.3, 4.9, and 4.4 kyrs. Wara et al. (2000) suggests that ice sheets are an important modulator of millennial scale oscillations and aid in developing high amplitude 5 kyr variability. Cortijo et al. (1995) suggests that the periodicities from 5-7 kyr that they detect in their sedimentary record are related to Heinrich event glacial oscillations. However, Ortiz et al. (1999) suggests that data from the western equatorial Atlantic indicates that periodicities from 4.8-6.1 kyr occur prior to intensification of Northern Hemisphere glaciation- thus implying that they could be related to a non-linear response to the harmonics of precession. Conversely, Steenbrink et al. (2003) argues that 5 kyr cyclicity is the result of combination tones of orbital signals.

6.2 Half and Quarter Precession: Evidence and Problems

This study shows that in the subtropical northwest Atlantic, half precessional variability (~11.5 kyr) is present in the initial insolation tuned age model and is expressed as a 12.5 kyr signal (see Table A.2). Existence of the 12.5 kyr signal in this region is consistent with the findings of Hagelberg et al. (1994), and Short et al. (1991). Observations by Hagelberg et al. (1994) of half precessional variability in the equatorial Atlantic and at high latitudes in the northeastern Atlantic, coupled with the completed data set in the subtropical northwest Atlantic, indicates that there may be communication up latitude via advective processes. This suggests that half precessional variability in this region is a non-linear response to orbital scale insolation forcing. However, this signal is only present in spectral analysis from 0-338 kyr and is absent from 338-875 kyr (Table A.2). The inconsistent presence of the half precessional signal despite a consistent precessional signal and changes in climate state leaves open the possibility that a non-linear response to variations in precession is not the sole contributor to the millennial-scale climate signal. Deviation from the expected half precessional signal may be due to inaccuracies based on the age model, as the ages between tie points are linearly interpolated creating an artificial, linear, sedimentation rate.

Fine tuning of the insolation based age model for the $\delta^{18}O$ record revealed inconsistencies in the position and power of the half and quarter precession signals (Table A.2). From 0-338 kyr the initial insolation tuned age model contained significant frequencies corresponding to climate signals at 23.1(>95% CI), 12.5, and 5.2 kyr (>90% CI). The second iteration of the insolation tuned age model from 0-338 kyr contained a significant precession peak at 23 kyr (>95% CI). The half precession signal shifted to an 11.6 kyr peak but is no longer of significant and no peaks occur at quarter precession (Table A.2).

In order to test the reproducibility of the periodicities present in the power spectrum of both time slices, (0-338 and 338-875 kyr) the initial spliced record was also tuned to an average global composite of 57 benthic $\delta^{18}O$ records from L&R 05. Comparison of the insolation based age models to the L&R 05 tuned age model demonstrates that the periodicities of millennial scale climate signals are age model dependent (Table A.2). This behavior has been observed in other studies targeted at exploring the accuracy of age model tuning which have determined that higher frequency signals are more susceptible to corruption from age model uncertainties (Huybers and Wunsch, 2004; Perron and Huybers, 2009). Proistosescu et al. (2012) found that orbitally tuned age models improves tests for distorted records with a strong orbital component and increases the significance of precession peaks while unturned records are better suited for detecting periodic variability in noisy records. The inconsistency in spectral power between age models and susceptibility to corruption brings detecting millennial scale variability using any single age model tuning method into question (Table A.2).

Data from spectral analysis of the insolation tuned record from 0-338 kyr and 338-875 kyr in the subtropical northwest Atlantic demonstrates a shift in dominant frequencies. During 0-338 kyr, the precessional cycle present occurs at 23.1 kyr. A 5.8 kyr quarter precession signal is expected for a 23 kyr periodicity.. Here, spectral analysis indicates its presence at 5.2 kyr, a difference which can be attributed to the age model (Table A.2). Analysis of the 338-875 kyr period contains two frequencies related to precession at 23.3 and 19.4 kyr. Resulting values for the quarter precession of 23 kyr periodicity occur at 5.9 and 5.3 kyr. For an expected precessional cycle of 19 kyr, the resulting quarter precession should occur at 4.8 kyr. Here they are found at 4.9 and 4.4 kyr (Table A.2). Due to the regional location of this study in the subtropical northwest Atlantic, it is unlikely that signals at this site are related to Heinrich event glacial oscillations (Cortijo et al., 1995). When only looking at the insolation based age model the differences in spectral power from 4-6 kyr for the two time slices, coupled with the changes in precessional cycles present, indicates the possibility of a non-linear link between precessional scale oscillations and events at higher frequencies.

A shift in power for quarter precessional periodicity occurs in both $\delta^{18}O$ time slices tuned to the L&R 05 benthic stack. The record from 0-338 kyr highlights the disappearance of the quarter precessional signal. The 338-900 kyr record contains signals of significant spectral power at 4.7, 4.5, and 4.2 kyr (Table A.2). These signals fall within bandwidth of the 18.1 kyr signal when interpreted as quarter precessional. Comparison between the age models makes it apparent that difference in tuning leads to significant varations at the millennial scale. Wunsch (2000) points out that aliasing is a problem in records looking at high frequency variation and that age interpolation injects false signals into the data set. Here, the reproduced record has a high enough sedimentation rate to make aliasing a non-issue. However, age model tuning using tie points assumes linear sedimentation rates between data points. This is problematic as periodicity timing is very sensitive to sedimentation rate; and assuming linear sedimentation rates implies a constant Δt.

This study has found similarities and differences in the timing and significance of millennial scale periodicity between the three age models. Presence and significance of 23 and 19 kyr precession peaks are consistent between all three age models (Table A.2). The timing and presence of half precession is inconsistent in the younger time slice of all three age models while in the older time slice the half precession signal is consistently missing (Table A.2). Quarter precession of the younger time slice between the three age models is inconsistent (Table A.2). However, quarter precession of the older time slice of all three age models can be considered somewhat consistent. The peaks are always present but the exact timing of the periodicities varies (Table A.2).

6.3 1.5 Kyr Peak

Numerous studies have indicated the presence of oscillations at millennial scale periodicities from 1.5 to 4 kyr (Bond et al., 1997; Schulz 2002; Dansgaard et al., 1997; Alley et al., 1999). While there is no currently accepted, clear, source for millennial scale climate change, several mechanisms causing fluctuations at these periods have been proposed. Wunsch (2000) proposes the problem of aliasing as a possible source for a 1.5 kyr signal; however with high enough sedimentation rates or proper recovery from ice cores this problem can be overcome. Alley et al. (1999) hypothesizes that climate change below 5 kyr is a product of quasi-periodic D/O events induced by changes in NADW production. He later proposed that the 1.5 kyr signal is a result of stochastic resonance induced by coupling of weak periodic forcing and noise from events related to ice sheets (Alley et al. 2001). Ekdahl et al. (2008) found that spectral power ranging from 1-1.7 kyr in their lake records from the South American Altiplano corresponded with a North Atlantic Hematite stained grain record reproduced by Bond et al. (2001) which suggests a high frequency forcing. Bond et al., (1997) suggests that the 1500 year periodicity results from changes in ocean and atmospheric circulation above Greenland. Comparing a speleothem $\delta^{18}O$ record to GISP 2 and GRIP cores, Clemens (2005) found evidence of two strong spectral peaks at ~1.7 and ~1.2 with a weak 1.5 kyr peak. Coupled with data from a ^{14}C record he concludes that millennial scale cyclicity derives from heterodynes of centennial scale solar activity which corroborate the findings from Bond et al. (2001). Other mechanisms that have been proposed include ice sheet dynamics (MacAyeal, 1993), or links between polar winds during the Holocene and deepwater fluctuations in the North Atlantic leading to thermohaline amplification (Oppo et al., 2003). Findings from Raymo et al. (2003) also indicate that warm temperatures have the potential to dampen high frequency variations on millennial timescales.

The insolation tuned data set analyzed in this study revealed high frequency oscillations that occur between ~1.5 – 4 kyr. As the regional study is located in the subtropical northwest Atlantic, it is unlikely that these signals directly derive from D/O or Heinrich events due to their isolation from waters in contact with glacial waters or IRD. It is also unlikely that the 1.5 kyr signal from 0-338 Ka is due to aliasing as the average time step is approximately 250 years. The L&R 05 tuned $\delta^{18}O$ data also contains significant strength above 95% at 1.5 kyr. This indicates that the 1.5 kyr signal is robust between age models even if peaks at the half and quarter precession are not (Table A.2). Changes in the age model affected peaks at half and quarter precession but did not affect the presence of the 1.5 kyr peaks. This implies that the signal controlling the 1.5 kyr peaks may derive from higher frequencies such as changes in atmospheric circulation induced by ice sheet dynamics or heterodynes of centennial scale solar activity.

Chapter 7

CONCLUSIONS

This study utilized $\delta^{18}O$ records from the white planktonic foraminiferal species, G*lobigerinoides ruber senso lato* as a proxy for sea surface hydrography. The site was located in the subtropical northwest Atlantic Ocean at Site 1059 and spanned the previously unstudied regional MIS 6-8. This record was spliced with other regional records in order to reproduce a continuous, high resolution $\delta^{18}O$ reconstruction for the past 900 kyr. The spliced record has a resolution sufficiently high enough to show millennial-scale variability in the region.

Spectral analysis of the initial insolation tuned record demonstrates sub-orbital oscillations at 12.5 kyr, ~4.5-6 kyr, and ~1.5-4 kyr. Comparison of the two spectral data sets (0-338 and 338-875) show changes in frequency based on presence of the precessional band. The younger data set has a 23 kyr periodicity with a corresponding half precession at 12.5 kyr and a 5.2 kyr signal representing the quarter precession. The older data set contains both a 23 and 19 kyr periodicity with signals at 5.9, 5.3, 4.9, and 4.4 kyr representing the quarter precession. However, the half precessional band is missing in the older data set.

Spectral analysis of the L&R 05 tuned record demonstrates inconsistencies in age model tuning, potentially inducing spurious significant results. Comparison of spectral results between the L&R 05 tuned record and insolation tuned record highlights this problem. The L&R 05 tuned record has a barely significant signal half precession peak at 11.6 kyr.while the younger time section from the insolation tuned age model falls at 12.5 kyr. The absence of a half precessional signal in the L&R 05 older time section is consistent with the insolation tuned time section. Spectral power for the quarter precession cycle also shifts between age models. The persistent occurrence of ~1.5 kyr spectral peaks between the two age models confirms that the signal is robust and not an artifact of the age models. I postulate that the ~1.5 kyr spectral peak is forced by events that occur at higher frequencies such as heterodynes of centennial solar variability or changes in atmospheric circulation patterns from ice sheet dynamics.

REFERENCES

Alley, R. B., P. U. Clark, L. D. Keigwin, and R. S. Webb (1999), Making sense of millennial-scale climate change, in *Mechanisms of Global Climate Change at Millennial Time Scales*, *Geophys. Monogr. Ser.*, vol. 112

Alley, R. B., Anandakrishnan, S., & Jung, P. (2001). Stochastic resonance in the North Atlantic. *Paleoceanography*, *16*(2), 190–198. doi:10.1029/2000PA000518

Anderson, M. (2001). Attenuation of millennial-scale events by bioturbation in marine sediments. *Paleoceanography*, *16*(4), 352-357.

Bemis, Bryan, E., Spero, Howard, J., Bijma, J., & Lea, David, W. (1998). Reevaluation of the oxygen isotopic composition of planktonic foraminifera: Experimental results and revised paleotemperature equations. *Paleoceanography*, *13*(2), 150–160.

Berger, A., Loutre, M. F., & Melice, J. L. (2006). Equatorial insolation: from precession harmonics to eccentricity. *Climate Of The Past*, 131–136.

Billups, K., Chaisson, W., Worsnopp, M., & Thunell, R. (2004). Millennial-scale fluctuations in subtropical northwestern Atlantic surface ocean hydrography during the mid-Pleistocene. *Paleoceanography*, *19*(2), PA2017. doi:10.1029/2003PA000990

Billups, K., Lindley, C., Fisler, J., & Martin, P. (2006). Mid Pleistocene climate instability in the subtropical northwestern Atlantic. *Global and Planetary Change*, *54*(3-4), 251-262. doi:10.1016/j.gloplacha.2006.06.025

Billups, K., Rabideaux, N., & Stoffel, J. (2011). Suborbital-scale surface and deep water records in the subtropical North Atlantic: implications on thermohaline overturn. *Quaternary Science Reviews*, *30*(21-22), 2976-2987. Elsevier Ltd. doi:10.1016/j.quascirev.2011.06.015

Bond, G., Broecker, W., Johnsen, S., McManus, J., Labeyrie, L., Jouzel, J., & Bonani, G. (1993). Correlations between climate records from North Atlantic sediments and Greenland ice. *Nature*, *365*(6442), 143-147. MACMILLAN MAGAZINES LTD. doi:10.1038/365143a0

Bond, G., Showers, W., Maziet, C., Lotti, R., Almasi, P., DeMenocal, P., Priore, P., et al. (1997). A Pervasive Millennial-Scale Cycle in North Atlantic Holocene and Glacial Climates. *Science*, *278*(5341), 1257–1266. doi:10.1126/science.278.5341.1257

Bond, G., Kromer, B., Beer, J., Muscheler, R., Evans, M. N., Showers, W., Hoffmann, S., et al. (2001). Persistent solar influence on North Atlantic climate during the Holocene. *Science (New York, N.Y.)*, *294*(5549), 2130–6. doi:10.1126/science.1065680

Broecker, W. S. (2000). Was a change in thermohaline circulation responsible for the Little Ice Age? *Proceedings of the National Academy of Sciences of the United States of America*, *97*(4), 1339-42. Retrieved from http://www.pubmedcentral.nih.gov/articlerender.fcgi?artid=34299&tool=pmcentrez&rendertype=abstract

Clemens, S. C. (2005). Millennial-band climate spectrum resolved and linked to centennial-scale solar cycles. *Quaternary Science Reviews*, *24*(5-6), 521–531. doi:10.1016/j.quascirev.2004.10.015

Cortijo, E., P. Yiou, L. Labeyrie, and M. Cremer (1995), Sedimentary record of rapid climatic variability in the North Atlantic Ocean during the Last Glacial Cycle, *Paleoceanography*, 10(5), 911–926, doi:10.1029/95PA02021.

Dansgaard, W., S. Johnsen, H. B. Clausen, D. Dahl-Jensen, N. Gunderstrup, C. U. Hammer, and Oeschger, H. (1984). North Atlantic climate oscillations revealed by deep Greenland ice cores, *Climate processes and climate sensitivity*, 288-298.

Droxler, A.; Farrell, J. (2000). Marine isotope stage 11 (MIS 11): New insights for a warm future. *Global and Planetary Change*, 1-5. Retrieved from http://www.mendeley.com/research/marine-isotope-stage-11-mis-11-new-insights-for-a-warm-future/

Ekdahl, E., Fritz, S. C., Baker, P., Rigsby, C., & Coley, K. (2008). Holocene multidecadal- to millennial-scale hydrologic variability on the South American Altiplano. *The Holocene*, *18*(6), 867–876. doi:10.1177/0959683608093524

Ferretti, P., Crowhurst, S. J., Hall, M. a., & Cacho, I. (2010). North Atlantic millennial-scale climate variability 910 to 790ka and the role of the equatorial insolation forcing. *Earth and Planetary Science Letters*, *293*(1-2), 28–41. doi:10.1016/j.epsl.2010.02.016

Flood, R. D., & Giosan, L. (2002). Migration history of a fine-grained abyssal sediment wave on the Bahama Outer Ridge. *Marine Geology*, *192*, 259–273.

Grützner, J., Giosan, L., Franz, S. ., Tiedemann, R., Cortijo, E., Chaisson, W. ., Flood, R. ., et al. (2002). Astronomical age models for Pleistocene drift sediments from the western North Atlantic (ODP Sites 1055–1063). *Marine Geology*, *189*(1-2), 5-23. doi:10.1016/S0025-3227(02)00320-1

Hagelberg, T. K., Bond, G., & deMenocal, P. (1994). Milankovitch band forcing of sub-Milankovitch climate variability during the Pleistocene. *Paleoceanography*, *9*(4), 545. doi:10.1029/94PA00443

Hagen, S., & Keigwin, L. D. (2002). Sea-surface temperature variability and deep water reorganisation in the subtropical North Atlantic during Isotope Stage 2–4. *Marine Geology*, *189*(1-2), 145-162. Elsevier. doi:10.1016/S0025-3227(02)00327-4

Healey, S., & Thunell, R. (2004). Millennial-scale variability in western subtropical North Atlantic surface and deep water circulation during marine isotope stages 11 and 12. *Paleoceanography*, *19*. doi:10.1029/2003PA000925

Heusser, L., & Oppo, D. (2003). Millennial- and orbital-scale climate variability in southeastern United States and in the subtropical Atlantic during Marine Isotope Stage 5: evidence from pollen and isotopes in ODP Site 1059. *Earth and Planetary Science Letters*, *214*(3-4), 483–490. doi:10.1016/S0012-821X(03)00389-3

Howell, P., Pisias, N., J Balance, J. Baughman, and L. Ochs, 2006. ARAND Time-Series Analysis Software, Brown University, Providence RI.

Huybers, P., & Wunsch, C. (2004). A depth-derived Pleistocene age model: Uncertainty estimates, sedimentation variability, and nonlinear climate change. *Paleoceanography*, *19*(1), n/a–n/a. doi:10.1029/2002PA000857

Hyde, W. T., & Crowley, T. J. (2002). Stochastic forcing of pleistocene ice sheets; implications for the origin of millennial-scale climate oscillations. *Paleoceanography*, *17*(4), 8-8. doi:http://dx.doi.org/10.1029/2001PA000669

Imbrie, J., D. Hays, D. G. Martinson, A. McIntyre, A. C. Mix, J. J. Morley, N. G. Paces, W. L. Prell, and N. J. Shackleton (1984). The orbital theory of Pleistocene climate: Support from a revised chronology of the marine $\delta^{18}O$ record. *Milankovitch and Climate*

Jouzel, J., Masson-Delmotte, V., Cattani, O., Dreyfus, G., Falourd, S., Hoffmann, G., Minster, B., et al. (2007). Orbital and millennial Antarctic climate variability over the past 800,000 years. *Science (New York, N.Y.)*, *317*(5839), 793-6. doi:10.1126/science.1141038

Keigwin, L. D., Rio, D., Acton, G. D., 1998. Proceedings of the Ocean Drilling Program, Initial Reports. Vol 172.

Kutzbach, J.E., Gallimore R., Harrison S.P., Behling, P., Selin, R. and Laarif F. (1998). Climate and biome simulations for the past 21,000 years. *Quaternary Science Reviews* 17(6-7): 473-506.

Kutzbach, J.E. and Guetter P.J. (1986). The influence of changing orbital parameters and surface boundary conditions on climate simulations for the past 18,000 years. *Journal of the Atmospheric Sciences*, 43(16), 1726-1759.

Laskar, J., Robutel, P., Joutel, F., Gastineau, M., Correia, A. C. M., & Levrard, B. (2004). A long-term numerical solution for the insolation quantities of the Earth. *Astronomy and Astrophysics*, *428*, 261–285. doi:10.1051/0004-6361

Lin, H.-L., Wang, W.-C., & Hung, G.-W. (2004). Seasonal variation of planktonic foraminiferal isotopic composition from sediment traps in the South China Sea. *Marine Micropaleontology*, *53*(3-4), 447-460. doi:10.1016/j.marmicro.2004.08.004

Lisiecki, L. E., and M. E. Raymo (2005), A Pliocene-Pleistocene stack of 57 globally distributed benthic $d^{18}O$ records, Paleoceanography, 20, PA1003, doi:10.1029/2004PA001071

Löwemark, L., Hong, W.-L., Yui, T.-F., & Hung, G.-W. (2005). A test of different factors influencing the isotopic signal of planktonic foraminifera in surface sediments from the northern South China Sea. *Marine Micropaleontology*, *55*(1-2), 49-62. doi:10.1016/j.marmicro.2005.02.004

MacAyeal, D.R. (1993). A low-order model of growth/purge oscillations of the Laurentide Ice Sheet, *Paleoceanograph*, 8, 767-773.

Margari, V., Skinner, L. C., Tzedakis, P. C., Ganopolski, a., Vautravers, M., & Shackleton, N. J. (2010). The nature of millennial-scale climate variability during the past two glacial periods. *Nature Geoscience*, *3*(2), 127-131. Nature Publishing Group. doi:10.1038/ngeo740

McManus, J., Oppo, D., & Cullen, J. (1999). A 0.5-million-year record of millennial-scale climate variability in the north atlantic. *Science (New York, N.Y.)*, *283*(5404), 971-5. Retrieved from http://www.ncbi.nlm.nih.gov/pubmed/9974387

Medina-Elizalde, M., Lea, D. W., & Fantle, M. S. (2008). Implications of seawater Mg/Ca variability for Plio-Pleistocene tropical climate reconstruction. *Earth and Planetary Science Letters*, *269*(3-4), 585-595. doi:10.1016/j.epsl.2008.03.014

Mudelsee, M., & Schulz, M. (1997). The Mid-Pleistocene climate transition: onset of 100 ka cycle lags ice volume build-up by 280 ka. *Earth and Planetary Science Letters*, *151*(1-2), 117-123. Elsevier. doi:10.1016/S0012-821X(97)00114-3

Oppo, D. W., Keigwin, L. D., McManus, J. F., & Cullen, J. L. (2001). Persistent suborbital climate variability in marine isotope stage 5 and termination II. *Paleoceanoghaphy*, *16*(3), 280-292.

Oppo, D. W., Linsley, B.K., Rosenthal, Y., Dannenmann, S., and Beaufort, L. (2003). Orbital and suborbital climate changes in the western tropical Pacific. *Geochemistry, Geophysics, Geosystems*, 4, doi: 10.1029/2002GC000260

Paul, A., Mulitza, S., Pätzold, J., & Wolff, T. (1999). Simulation of Oxygen Isotopes in a Global Ocean Model, 655-686.

Perron, J. T., and Huybers, P. (2009) Is there an orbital signal in the polar layered deposits on Mars? , *Geology*,

Pestiaux, P., Van der Mersch, I., Berger, A., and Duplessy, J. C. (1988). Paleoclimate variability at frequencies ranging from 1 cycle per 10000 years to 1 cycle per 1000 years: Evidence for non-linear behaviour of the climate system. *Climate Change*, 12, 9-37.

Proistosescu, C., Huybers, P., & Maloof, A. C. (2012). To tune or not to tune: Detecting orbital variability in Oligo-Miocene climate records. *Earth and Planetary Science Letters*, *325-326*, 100–107. doi:10.1016/j.epsl.2012.01.022

Prothero, D. (1998). *Bringing Fossils to Life: An Introduction to Paleobiology*. McGraw-Hill Companies.

Raymo, M. E. (2004). Stability of North Atlantic water masses in face of pronounced climate variability during the Pleistocene. *Paleoceanography*, *19*(2), PA2008. doi:10.1029/2003PA000921

Reiter, P. (2000). From Shakespeare to Defoe: malaria in England in the Little Ice Age. *Emerging infectious diseases*, *6*(1), 1-11. Retrieved from http://www.pubmedcentral.nih.gov/articlerender.fcgi?artid=2627969&tool=pmcentrez&renrendert=abstract

Ryan, W. B. F., et al. (2009), Global Multi-Resolution Topography synthesis, Geochem. Geophys. Geosyst., 10, Q03014, doi:10.1029/2008GC002332.

Ruddiman, W. F. (2001). *Earth's Climate: Past and Future*. W. H. Freeman.

Rutherford, S., & D'Hondt, S. (2000). Early onset and tropical forcing of 100,000-year Pleistocene glacial cycles. *Nature*, *408*(6808), 72-5. doi:10.1038/35040533

Schulz, M. (2002). On the 1470-year pacing of Dansgaard-Oeschger warm events. *Paleoceanography*, *17*(2), 4–1–4–9. doi:10.1029/2000PA000571

Schulz M, Mudelsee M (2002) REDFIT: Estimating red-noise spectra directly from unevenly spaced paleoclimatic time series. *Computers and Geosciences* 28:421–426.

Shackleton, N. J., Backman, J., Zimmerman, H., & Et Al. (1984). Oxygen isotope calibration of the onset of ice-rafting and history of glaciation in the North Atlantic region. *Nature*, *307*(5952), 620-623. Nature Publishing Group. Retrieved from http://academiccommons.columbia.edu/download/fedora_content/download/ac:143644/CONTENT/307620a0.pdf

Short, D. A., Mengel, J. G., Crowley, T. J., Hyde, W. T., & North, G. R. (1991). Filtering of Milankovitch Cycles by Earth's Geography. *Quaternary Research, 35*, 157-173.

Steenbrink, J., Kloosterboer-van Hoeve, M. L. and Hilgen, F.J., (2003). Millennial-scale climate variations recorded in Early Pliocene colour reflectance time series from the lacustrine Ptolemais Basin (NW Greece). *Global and Planetary change*, 36: 47-75.

Van Geel, B., Raspopov, O. M., Renssen, H., Van der Plicht, J., Dergachev, V. a., & Meijer, H. a. J. (1999). The role of solar forcing upon climate change. *Quaternary Science Reviews*, *18*(3), 331–338. doi:10.1016/S0277-3791(98)00088-2

Wang, L. (2000). Isotopic signals in two morphotypes of Globigerinoides ruber (white) from the South China Sea: implications for monsoon climate change during the last glacial cycle. *Palaeogeography, Palaeoclimatology, Palaeoecology*, *161*(3-4), 381-394. doi:10.1016/S0031-0182(00)00094-8

Wara, M. W., Ravelo, A. C., & Revenaugh, J. S. (2000). The Pacemaker always rings twice. *Paleoceanography*, *15*(6), 616–624.

Weirauch, D., Billups, K., & Martin, P. (2008). Evolution of millennial-scale climate variability during the mid-Pleistocene. *Paleoceanography*, *23*(3), 1-16. doi:10.1029/2007PA001584

Wunsch, C. (2000). On sharp spectral lines in the climate record and the millennial peak. *Paleoceanography*, *15*(4), 417–424.

Yokokawa, M., & Franz, S.-O. (2002). Changes in grain size and magnetic fabric at Blake–Bahama Outer Ridge during the late Pleistocene (marine isotope stages 8–10). *Marine Geology*, *189*(1-2), 123–144. doi:10.1016/S0025-3227(02)00326-2

Appendix A

TABLES

Table A.1: Summary of site locations and data source references

Reference	Age (Ka)	Species	Site	Lat/Long (°)
Hagen & Keigwin, 2002	0-76	G. ruber s.s. and s.l.	1059	31N/75W
Heusser et al., 2003	57-269	G. ruber s.s. and s.l.	1059	31N/75W
this study	127-266	G. ruber s.l.	1059	31N/75W
Billups et al., 2011	262-339	G. ruber s.l.	1056	32N/76W
Billups et al., 2004	339-459	G. sacc	1056	32N/76W
Weirauch et al., 2008	413-1352	G. ruber s.l.	1058	32N/75W

Table A.2: Summary of significant peaks and persistence between age models

		Precession 23 kyr	**Precession 19 kyr**	**Half precession**	**Quarter precession**	**1.5 kyr 0-338 Ka**
Insol. V. 1	0-338	23.1	N/A	12.5	5.2, 4.8	~1.6
	338-875	23.3	19.4	N/A	5.9, 5.3, 4.9, 4.4	
Insol. V.2	0-338	23	N/A	N/A	N/A	~1.6
	338-875	22.9	19.1	N/A	5.9, 5.1	
L&R 05	0-338	23.1,	N/A	11.6	N/A	~1.5
	338-875	23.3	18.1	N/A	N/A 4.7, 4.5, 4.2	
		Consistent	Consistent	Inconsistent	Consistent	Consistent

Appendix B

FIGURES

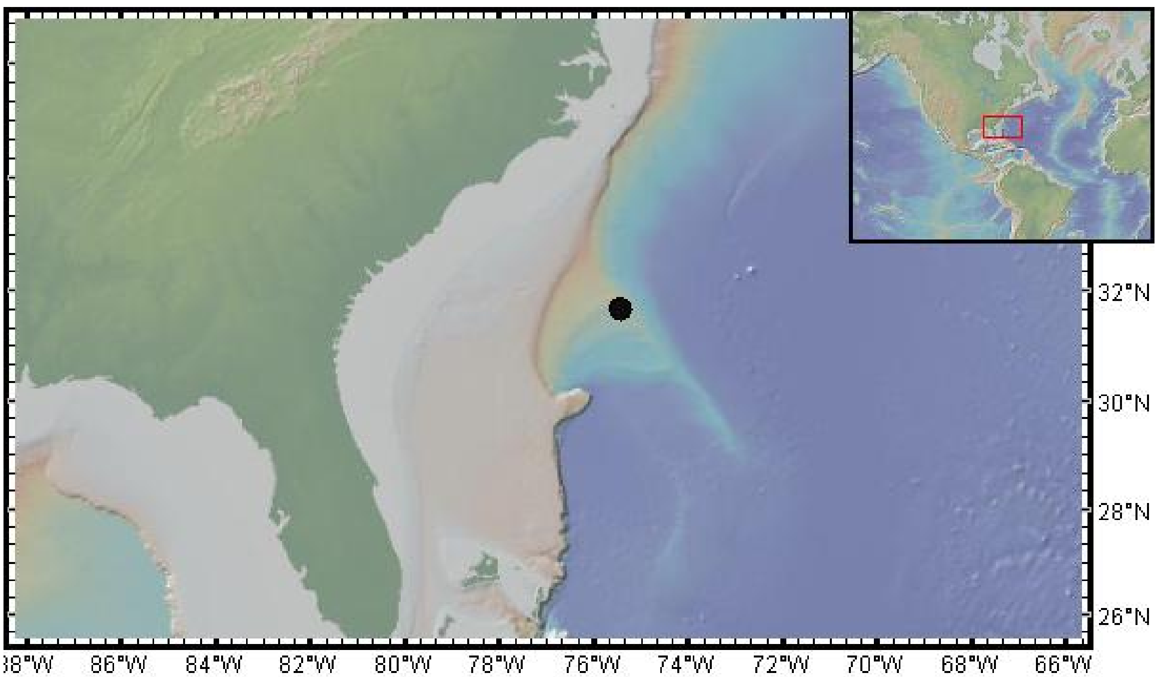

Figure B.1: Location of ODP Site 1059 in the northwestern subtropical Atlantic Ocean (31°40.461’N, 75°25.127’W) at 2985 meters depth. Created using GeoMapApp (http://www.geomapapp.org)

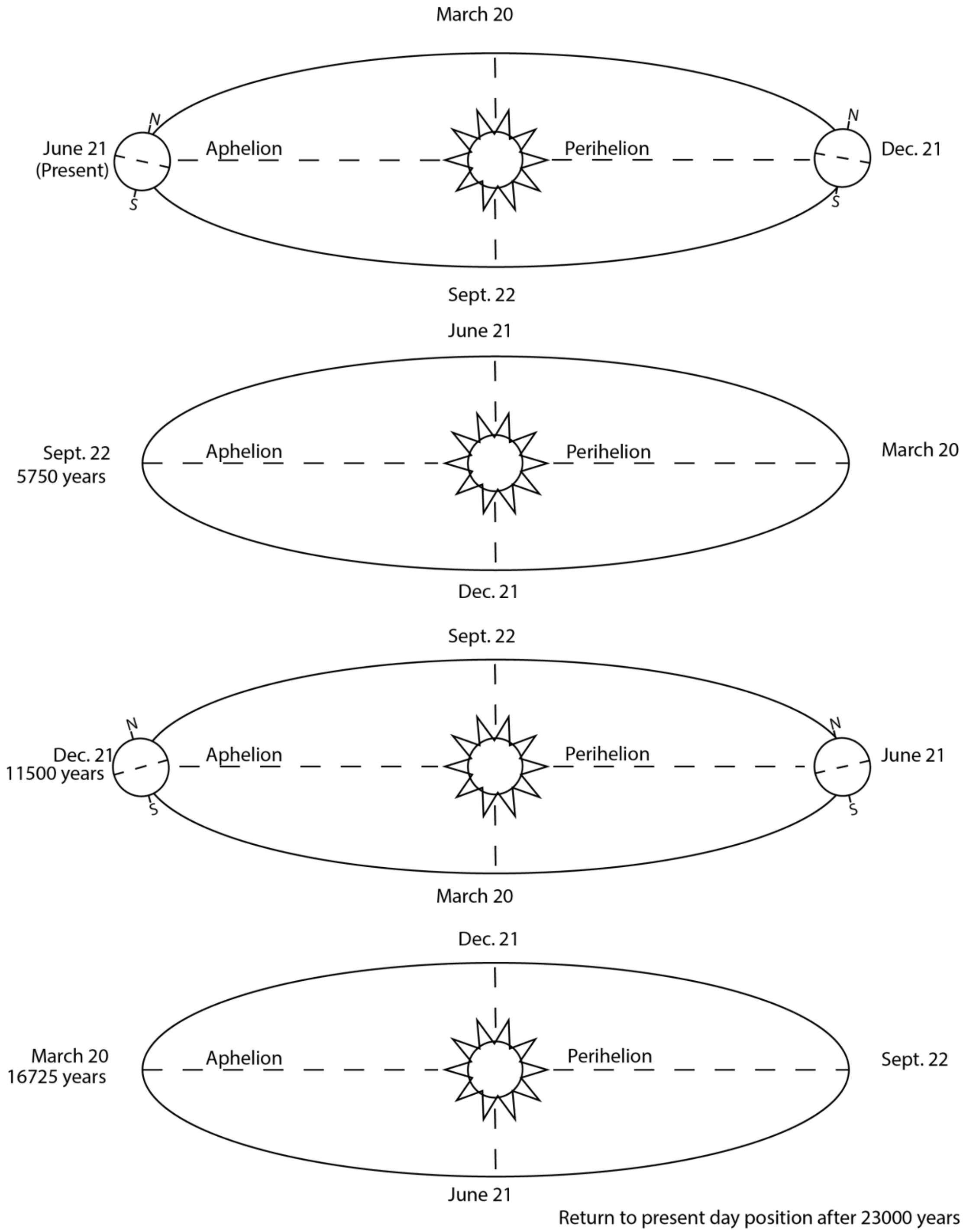

Figure B.2: Combined motion of axial precession and precession of the ellipse (Adapted from Ruddiman 2001). Precessional changes in the direction of Earth's spin axis coupled with elliptical precession produce changes in the distance, timing, and hemispheric position between Earth and the Sun.

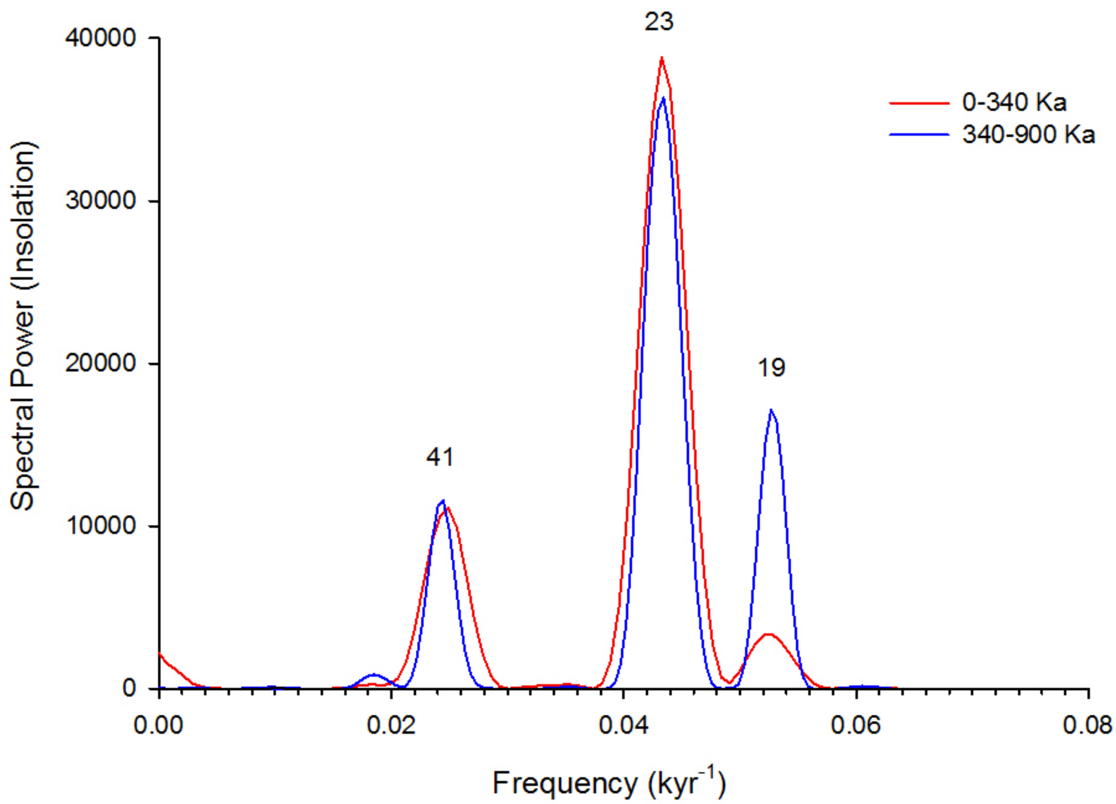

Figure B.3: Spectral analysis of Northern Hemisphere insolation (Laskar, 2004) from 0-340 and 340-900 Ka. In the younger time segment there is a strong spectral peak corresponding to a 23 kyr periodicity and a weak 19 kyr peak. The older time segment has strong 23 and 19 kyr spectral peaks. Time series analysis was conducted using the Arand software package (Howell et al., 2006).

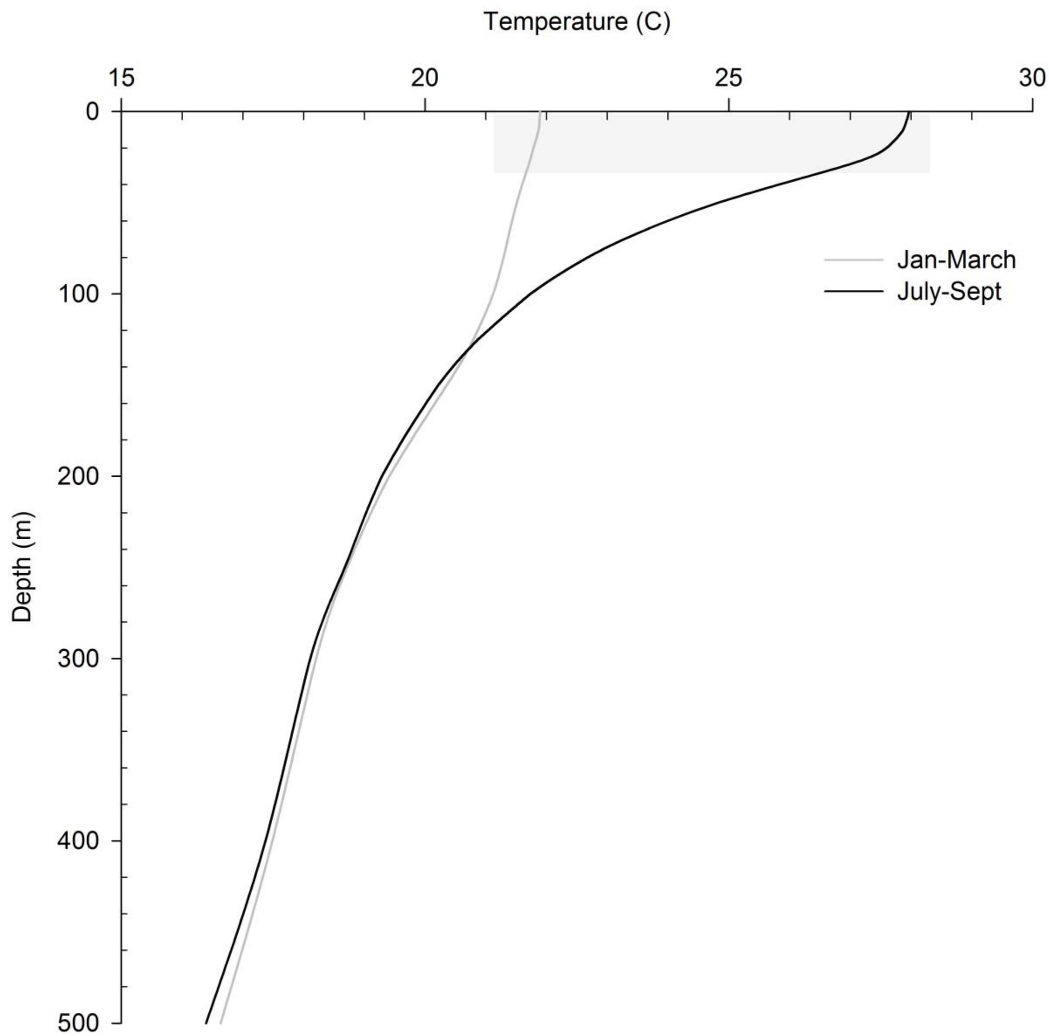

Figure B.4: Seasonal upper ocean temperature profile at Site 1059 created using Levitus 1994. The box denotes the depth range of *G. ruber*. Temperatures are cooler in the top 100m during the winter and warm during the summer months with a 6ºC difference between seasons.

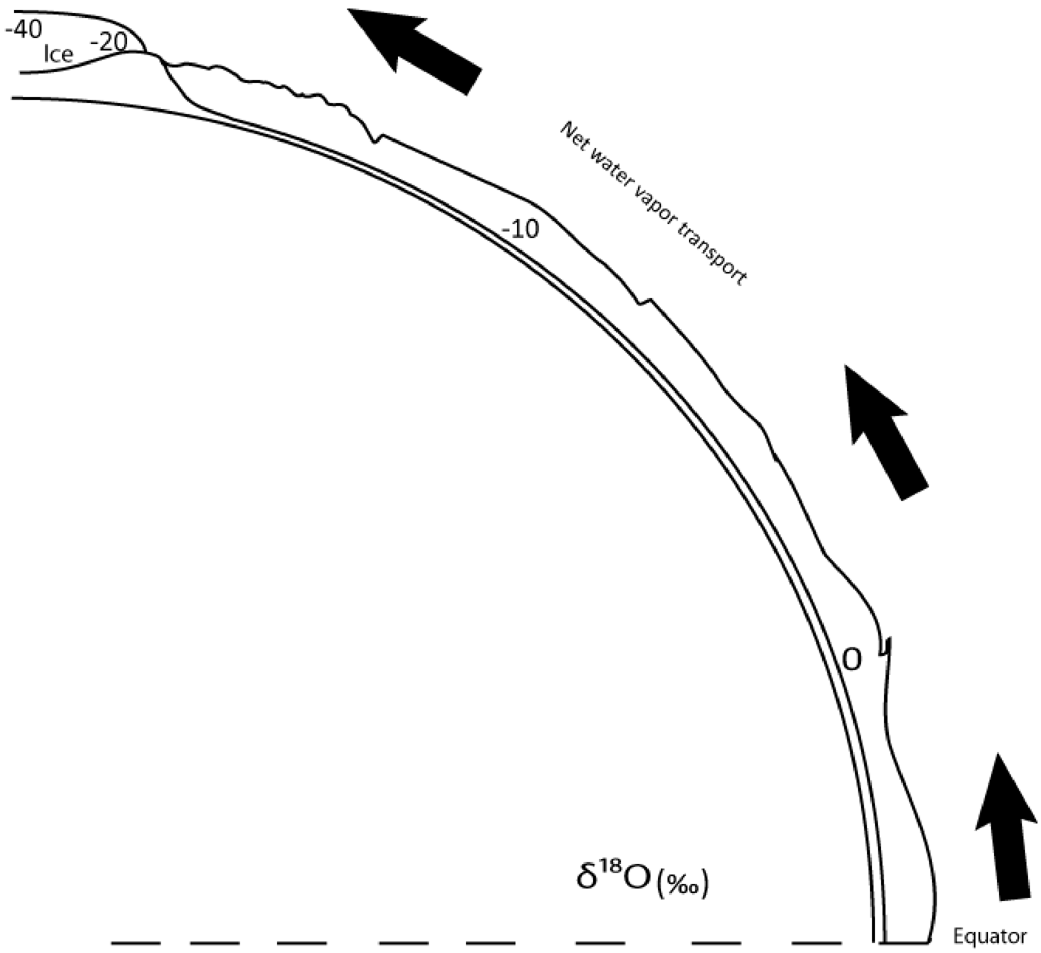

Figure B.5: General Rayleigh distribution model of $\delta^{18}O$ values. Water vapor moving from the tropics to the poles is enriched in ^{16}O due to evaporation and condensation processes.Water vapor isotope fractionation makes the $\delta^{18}O$ values of polar condensation negative

.

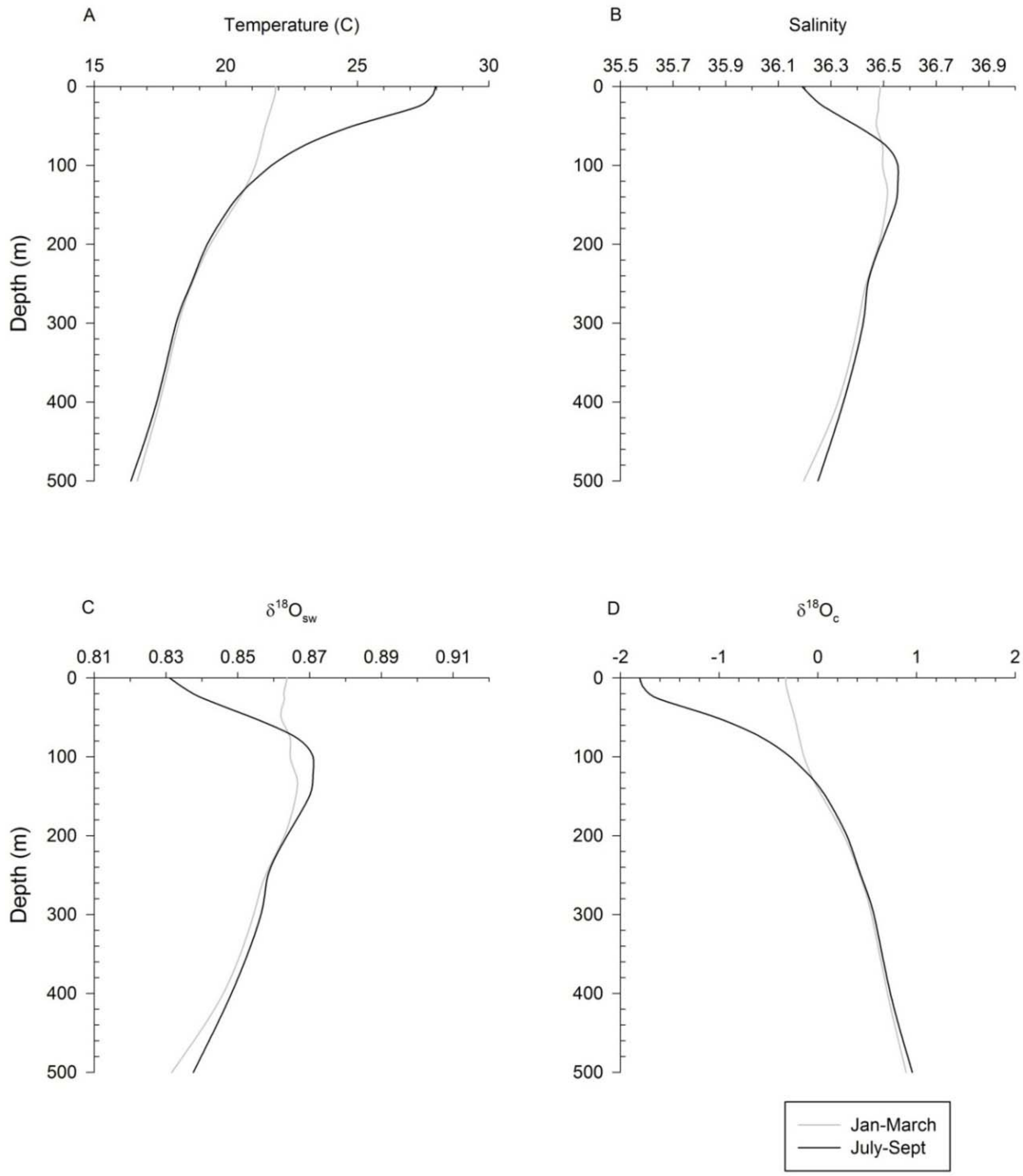

Figure B.6: (A) Resized graph from Figure B.2 showing temperature with depth. (B) Seasonal salinity with depth. (C) δ^{18}O of seawater (sw) calculated based on seasonal salinity values. (D) Difference in seasonal δ^{18}O of equilibrium calcite (c) based on seasonal salinity and temperature.

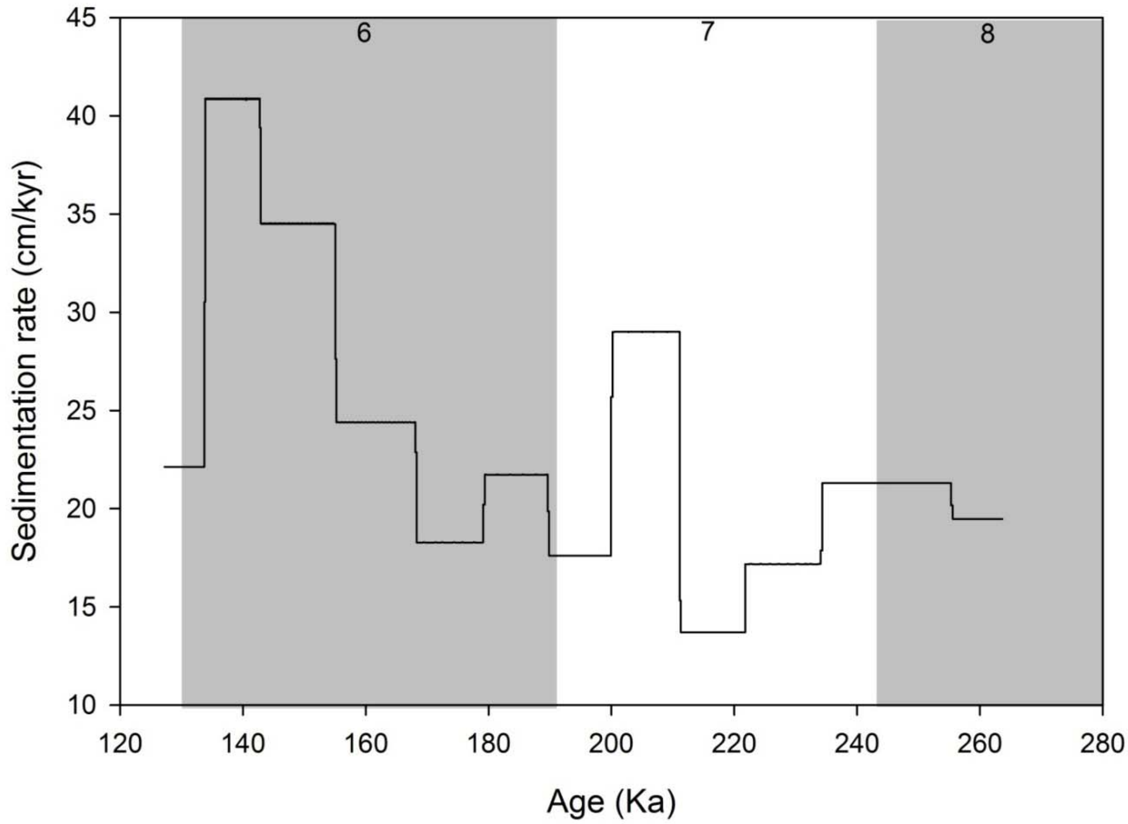

Figure B.7: Calculated sedimentation rates for Site 1059 from 129 Ka to 267 Ka based on the Grützner et al. (2002) age model. High sedimentation rates coincide with glacial intervals and lower rates with interglacial. Average time step between samples in the record is 200 years.

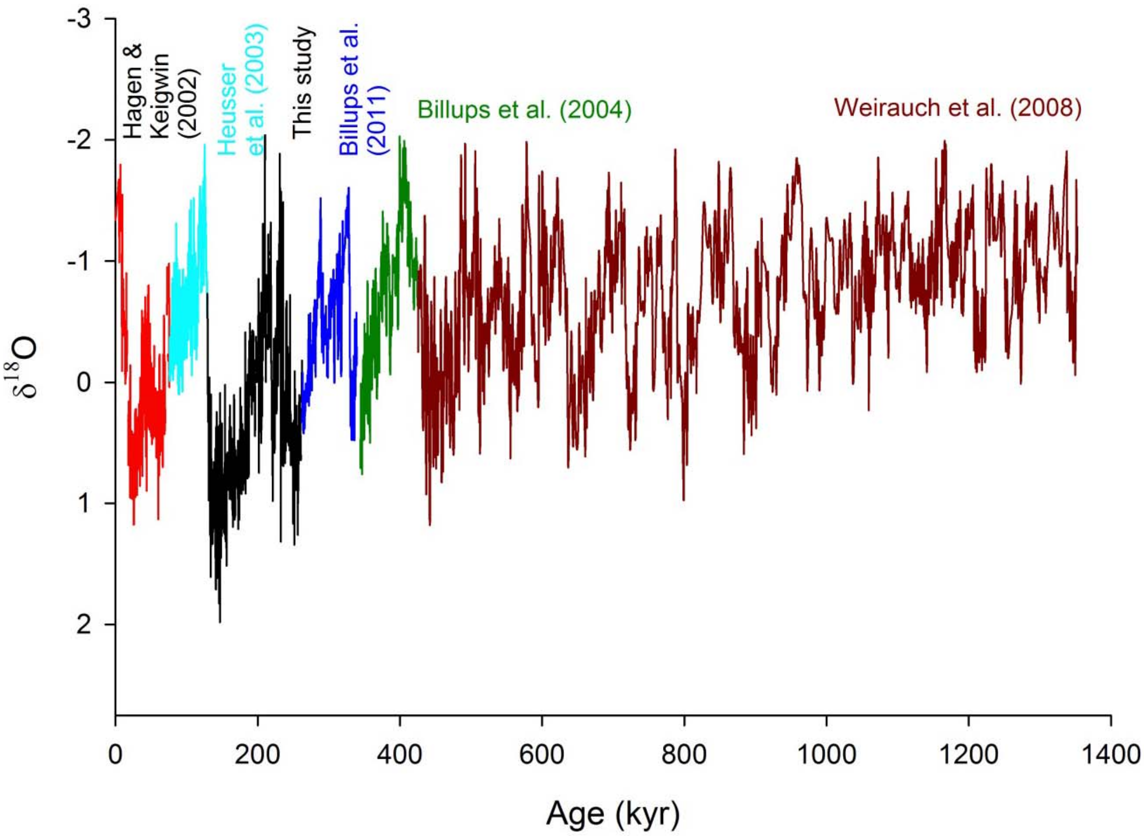

Figure B.8: Record splicing of the subtropical northwest Atlantic regional studies to create a continuous high resolution $\delta^{18}O$ record. See Table A.1 for study descriptions.

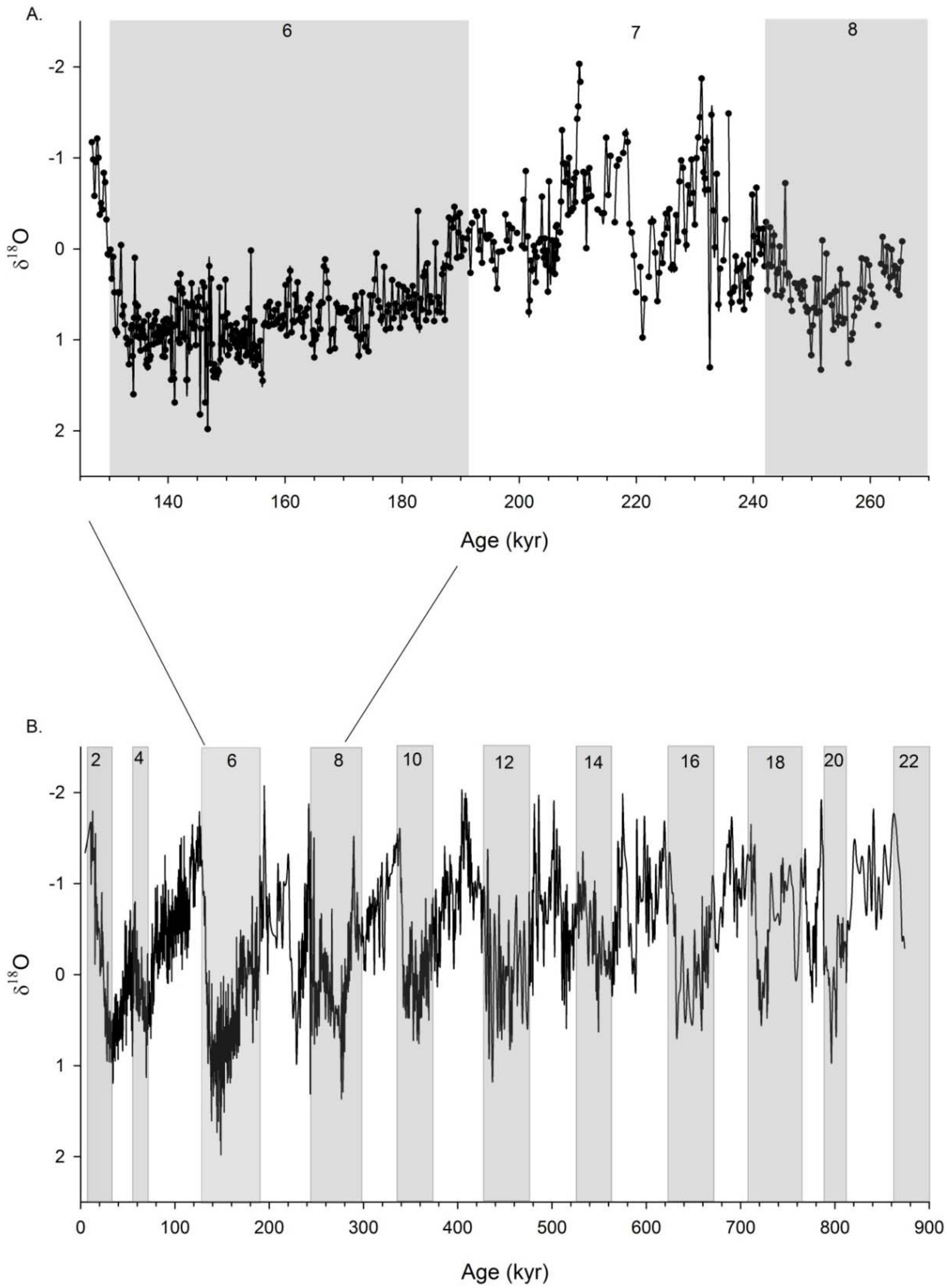

Figure B.9: (A) Reproduced δ^{18}O record for this study with two glacial intervals (MIS 6,8) and one interglacial (MIS 7). (B) Regional composite of Subtropical northwest Atlantic δ^{18}O records. Marine Isotope Stages are numbered in both graphs.

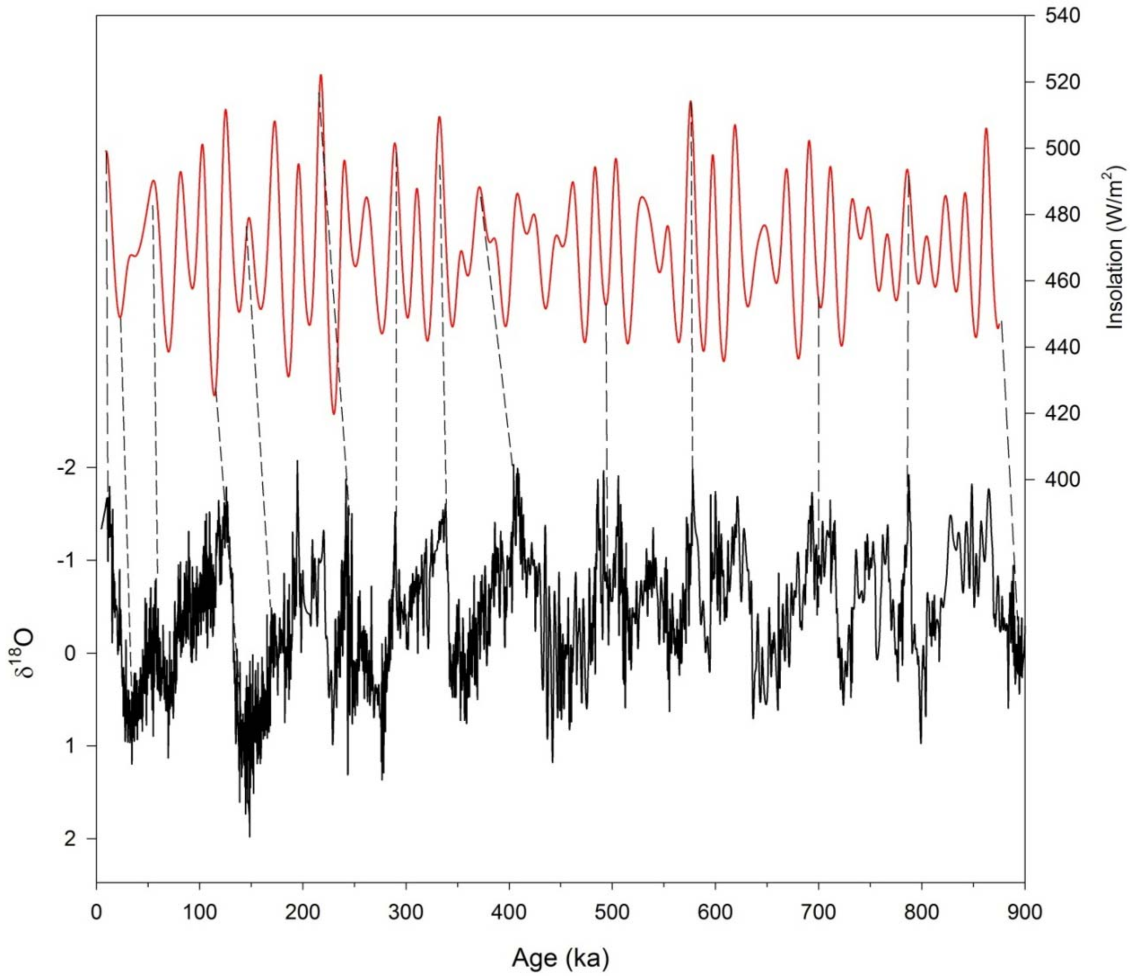

Figure B.10: Tuning of the $\delta^{18}O$ record to northern hemisphere insolation (Lasker, 2004). The dashed lines represent example tie points that were used to shift the regionally spliced $\delta^{18}O$ record to match insolation.

A.

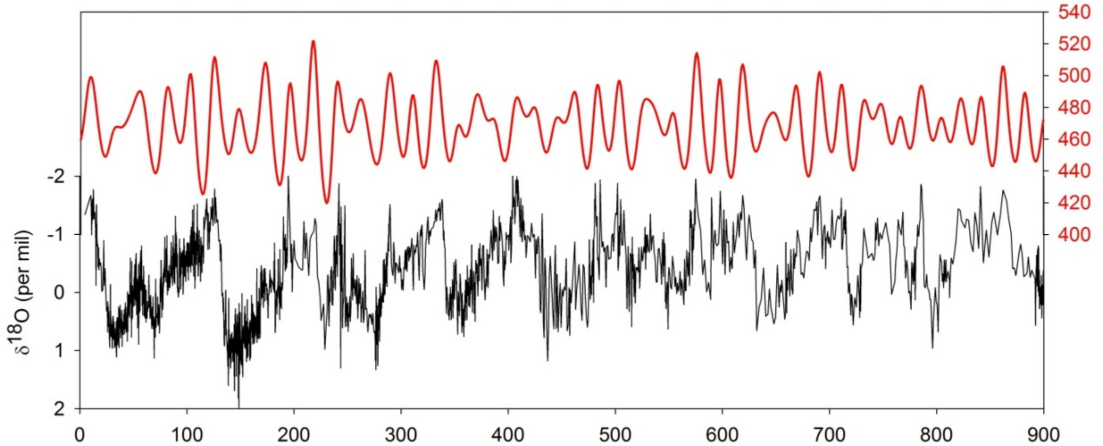

B.

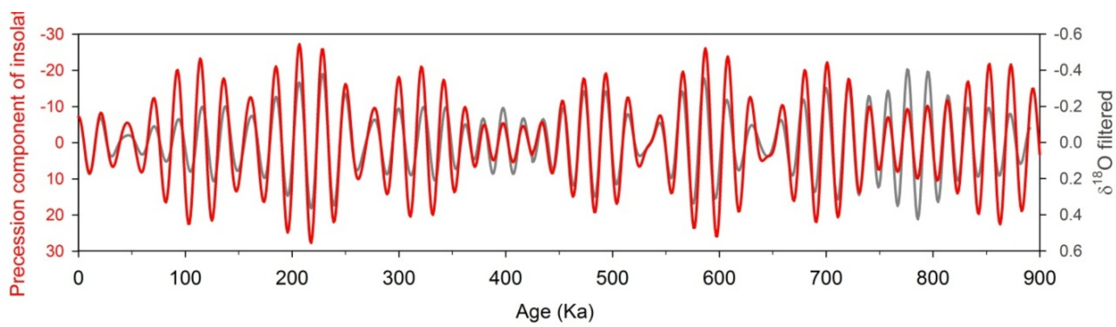

Figure B.11: (A) Spliced δ^{18}O time series tuned to insolation (Laskar, 2004). (B) Filtered δ^{18}O signal centered on 20 kyr compared to precession. Overall periodicity and amplitude of the records fit well. A poor fit in amplitude between the two records occurs from 750 to 800 Ka.

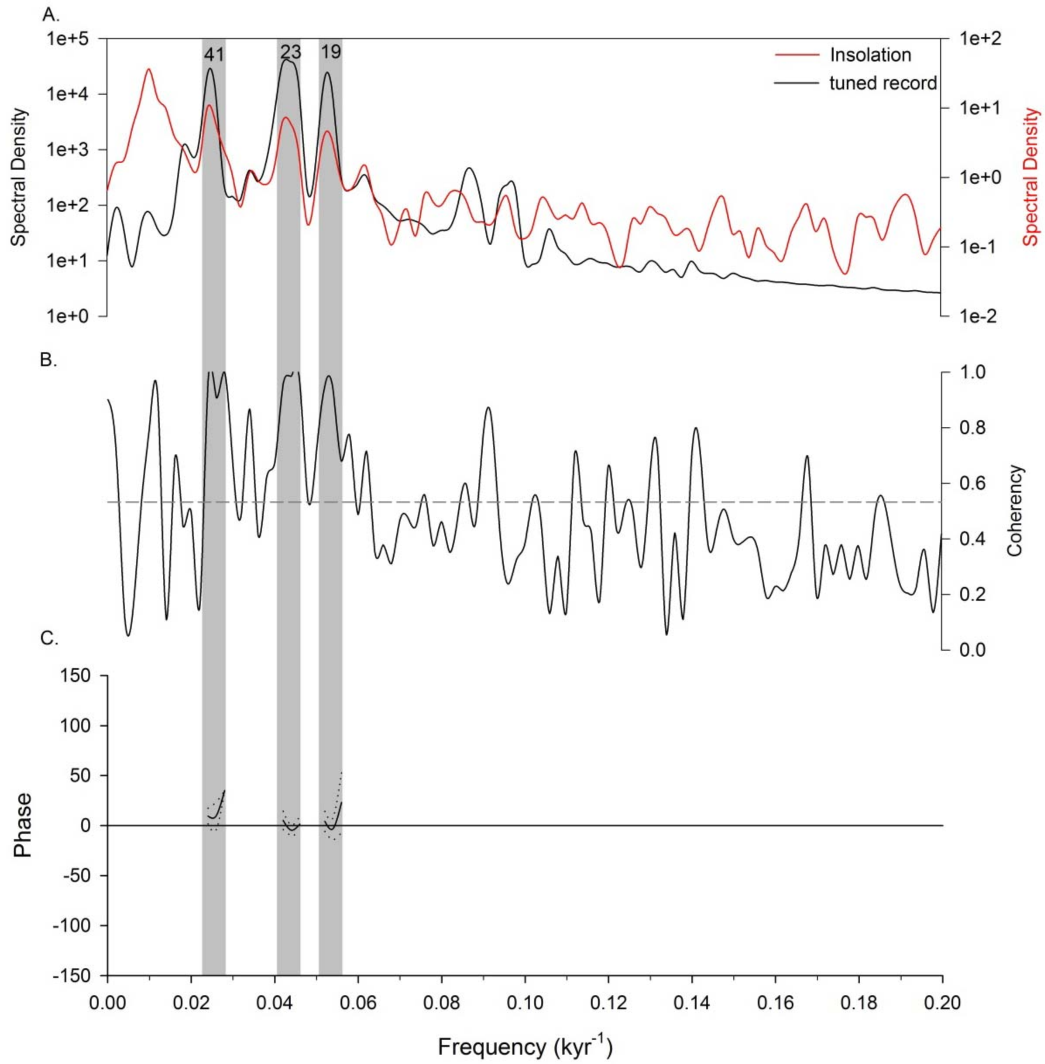

Figure B.12: Cross Spectral Analysis of the initial insolation tuned age model. (A) The 41, 23, and 19 kyr periodicities have strong peaks and (B) high coherence (k>90) between the two records occurs in the obliquity and precession peaks. (C) Phase plots (black) and error bars (dotted line) indicate alignment of peaks between both time series. The obliquity peaks are out of phase by 2.1 kyr. The 23 kyr peaks are in phase. The 19 kyr peaks are out of phase by 428 years, but based on the plotted error bars, can be considered in phase.

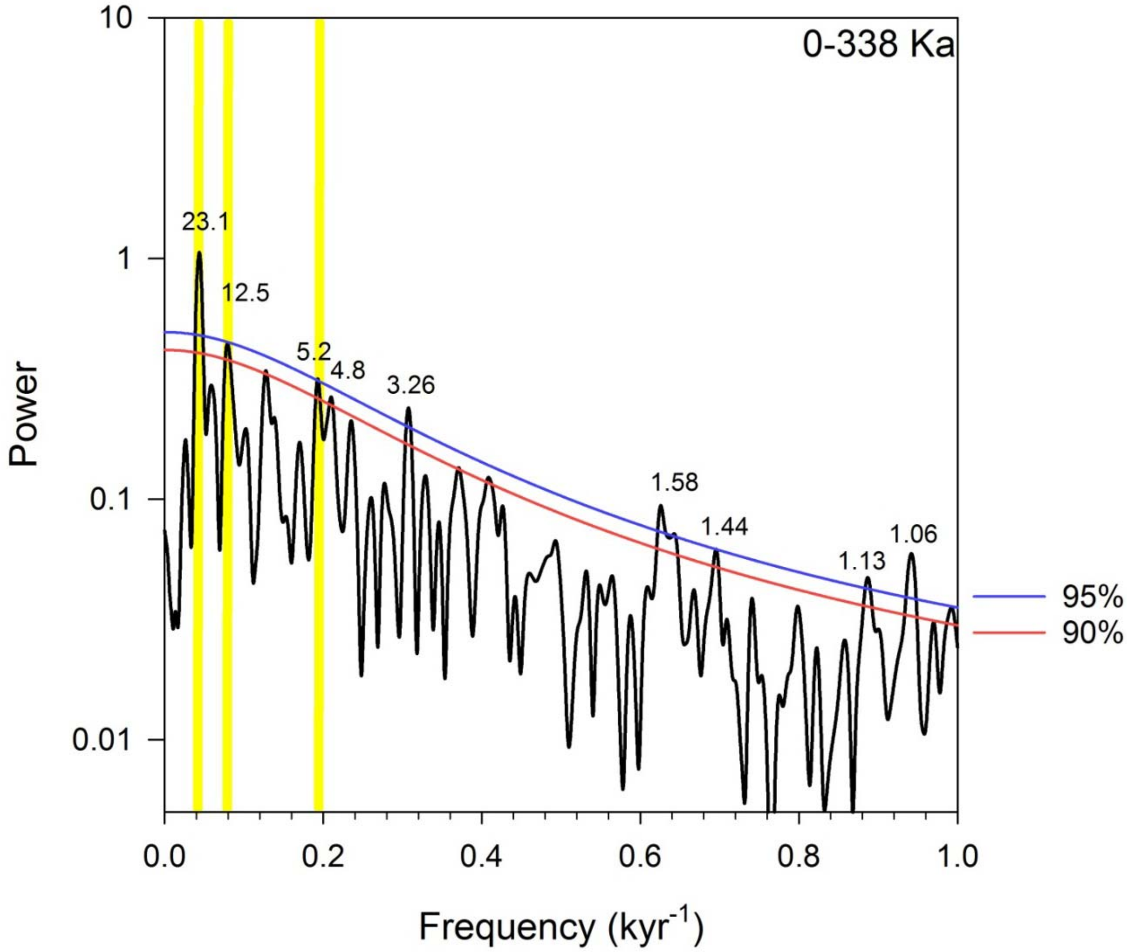

Figure B.13: Spectral analysis of the spliced $\delta^{18}O$ record in the subtropical northwestern Atlantic from 0-338 Ka based on the initial insolation based age model. The record was high-pass filtered to remove periods longer than 33 kyr. The suborbital periodicities at 12.5 kyr and 5.2 kyr are close to half and quarter precession cycles of the 23 kyr signal (within bandwidth). The time step is 250 years, and significant periodicities in the 1-1.5 kyr band are also apparent.

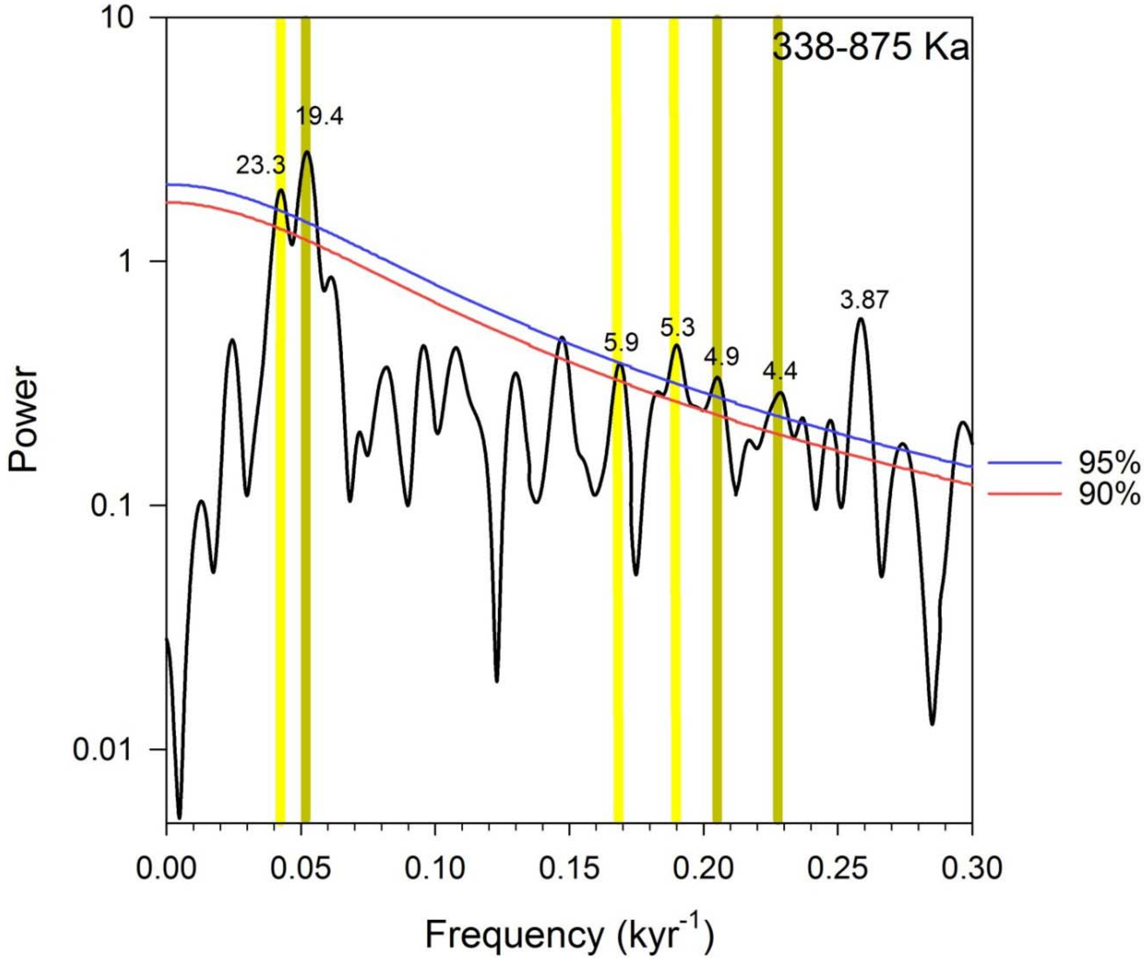

Figure B.14: Spectral analysis of the spliced (and filtered) δ^{18}O record from 338-875 Ka using the initial insolation based age model. In addition to the quarter precession peaks related to the longer, 23 kyr precession cycle (5.9 kyr and 5.3 kyr), higher frequencies that are more closely related to quarter precession cycles of the 19 kyr precession cycle are also present (4.9 kyr, 4.4 kyr). No half precession cycle is observed. The time step is 450 years, and higher frequency cycles are not resolved.

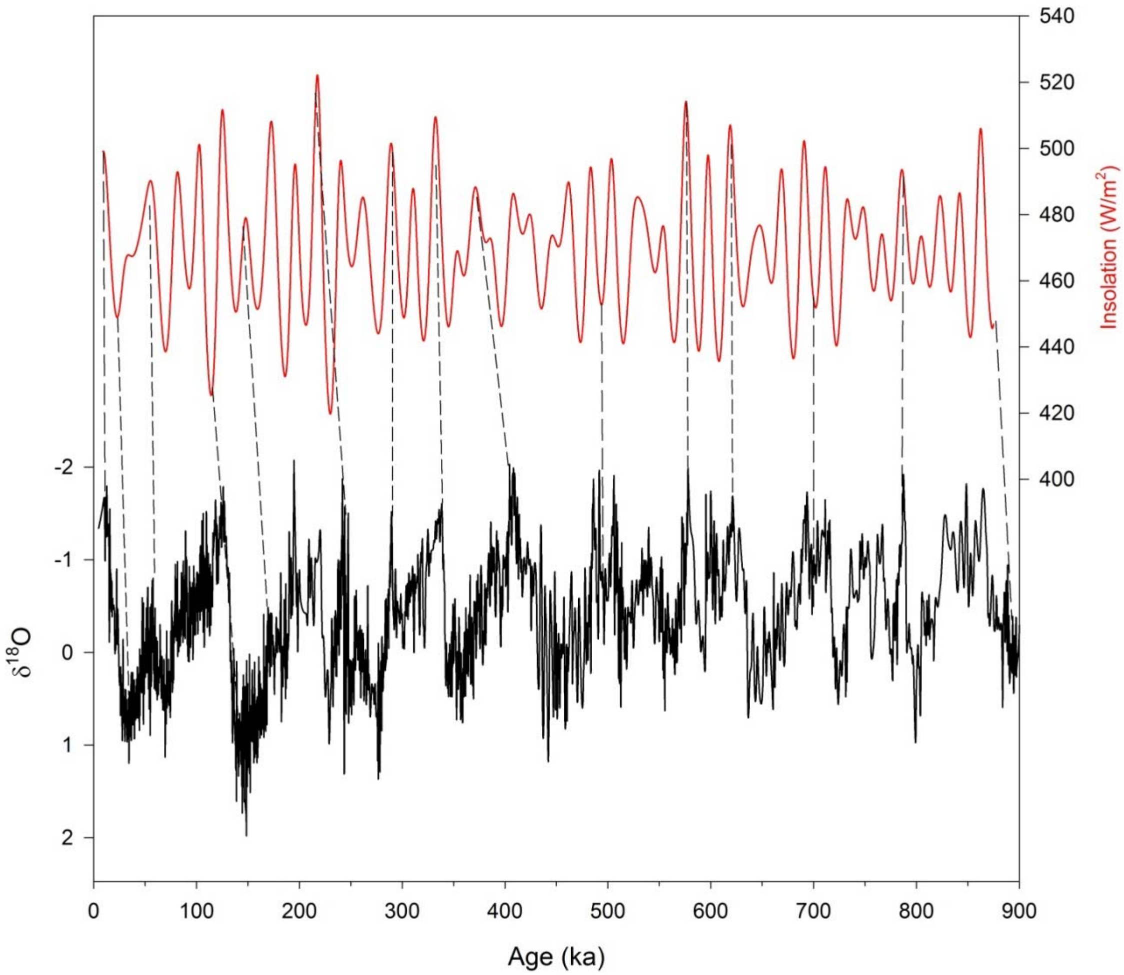

Figure B.15: Second version tuning attempt of the unturned $\delta^{18}O$ record to northern hemisphere insolation (Lasker, 2004). The dashed lines represent example tie points used to shift the $\delta^{18}O$ record to match insolation.

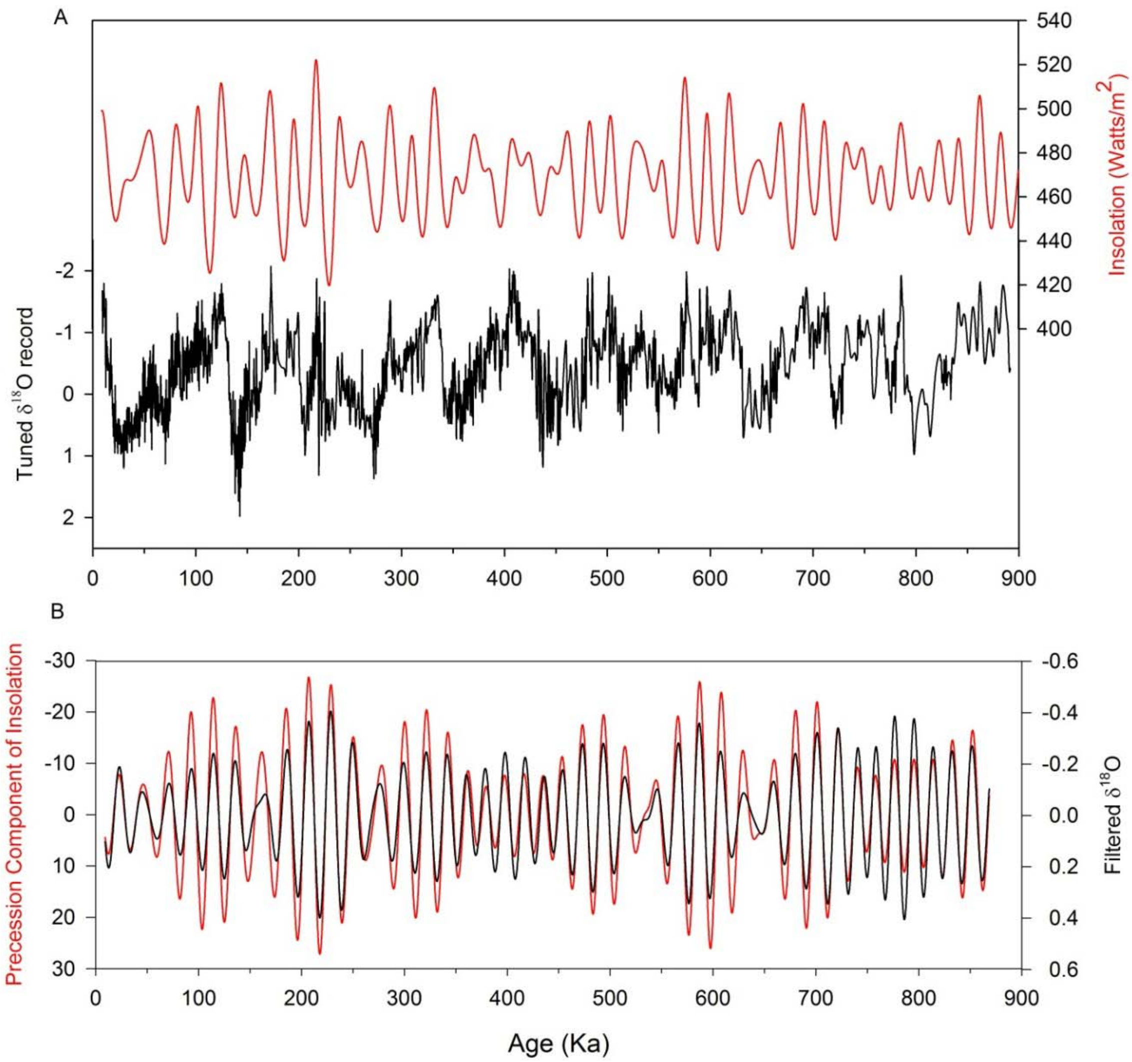

Figure B.16: (A) The black line represents the record resulting from the second tuning to the insolation record (red line). (B) Comparison of the two records filtered to show the precession component of insolation. The periodicity of the tuned record does not quite match with precession at approximately 150 Ka and 650 Ka. The amplitude of the adjusted record fits well with the precession component of insolation from 350 to 500 Ka. There is a mismatch in amplitude from 750 to 800 Ka.

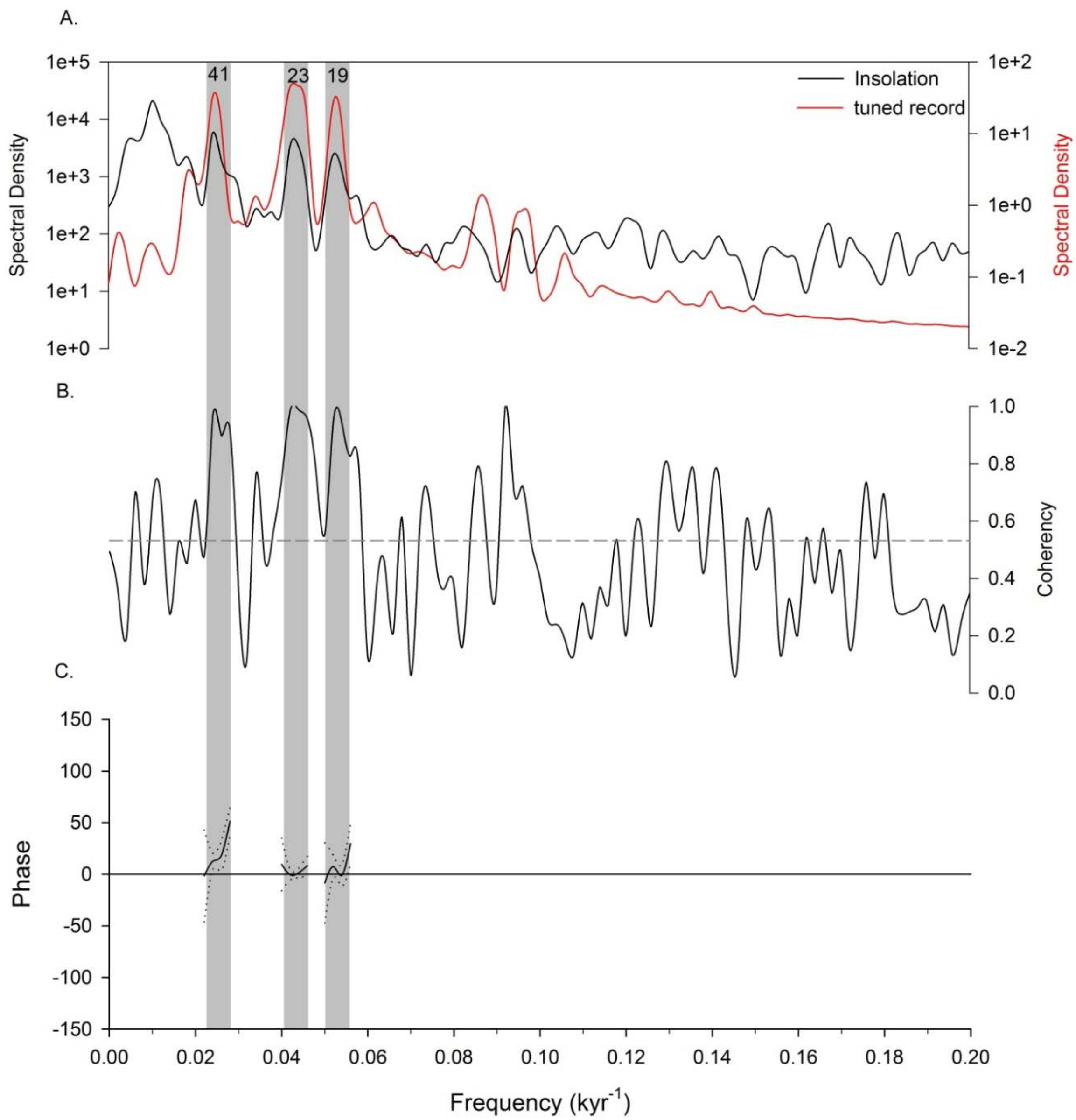

Figure B.17: Cross Spectral Analysis of the second insolation based age model. (A) The 41, 23, and 19 kyr periodicities have strong peaks and (B) high coherence between the two records occur at all three orbital cycles (41, 23, and 19 kyr). (C) Phase plots (black) and error bars (dotted line) indicates alignment of peaks between both time series. The obliquity peaks are out of phase by 2.3 kyr. The 23 and 19 kyr peaks are out of phase by 319 and 369 years, respectively. However, based on the error bars the 23 kyr peak can be considered to be in phase. The skewed phases indicate a poor age model fit.

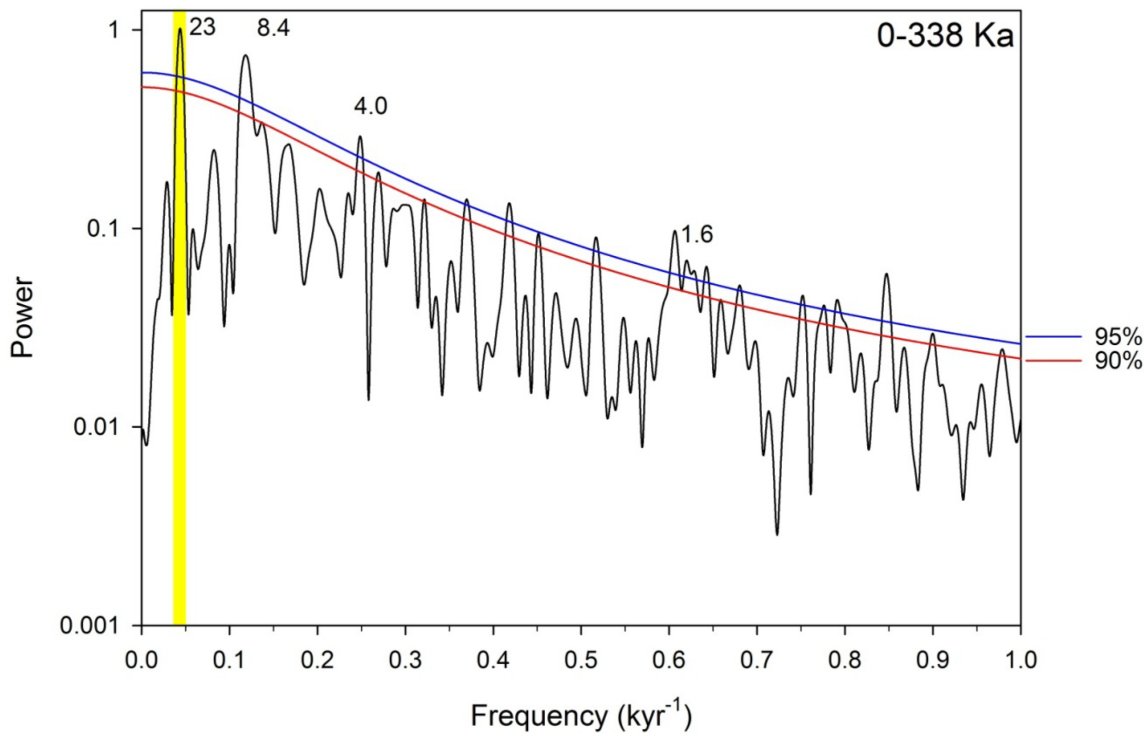

Figure B.18: Spectral analysis of the second insolation based age model (0-338 Ka). A precessional peak occurs at 23 kyr above a 95% confidence. The 11.6 kyr peak is not significant. An 8.4 kyr peak occurs well above the 95% confidence interval and is almost as powerful as the precessional peak. Signals at the quarter precession are not present, but 3 peaks with an average value of 1.6 kyr occur above the 95% confidence interval.

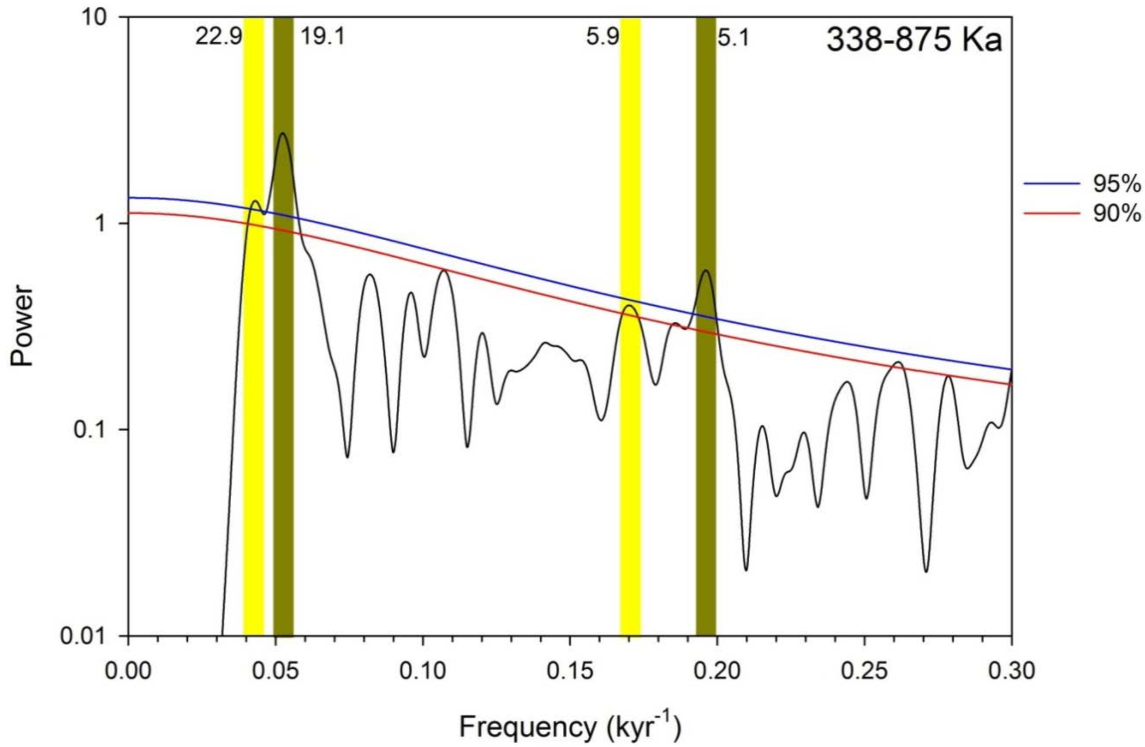

Figure B.19: Spectral analysis of the second insolation based age model (338-875 Ka). Two precessional peaks occur above 95% confidence at 22.9 and 19.1 kyr. No half precession signal is present. The 5.9 kyr peak may be related to the quarter precession of the 22.9 kyr precession peak and the 5.1 kyr related to the quarter precession of the 19.1 kyr precession peak.

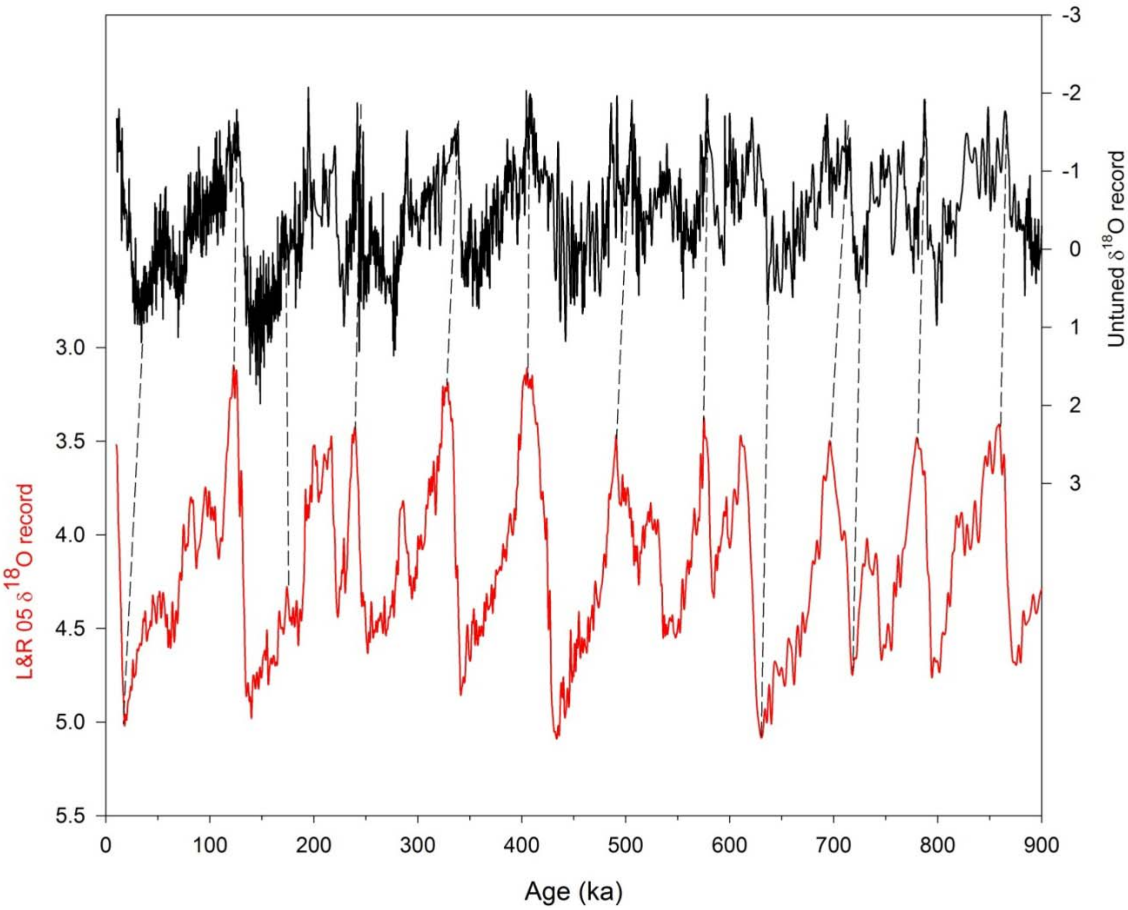

Figure B.20: Age model tuning of the untuned δ^{18}O record using the Lisiecki and Raymo (2005) benthic δ^{18}O stack. The dashed lines represent example tie points that were used to shift the δ^{18}O record to match the benthic stack.

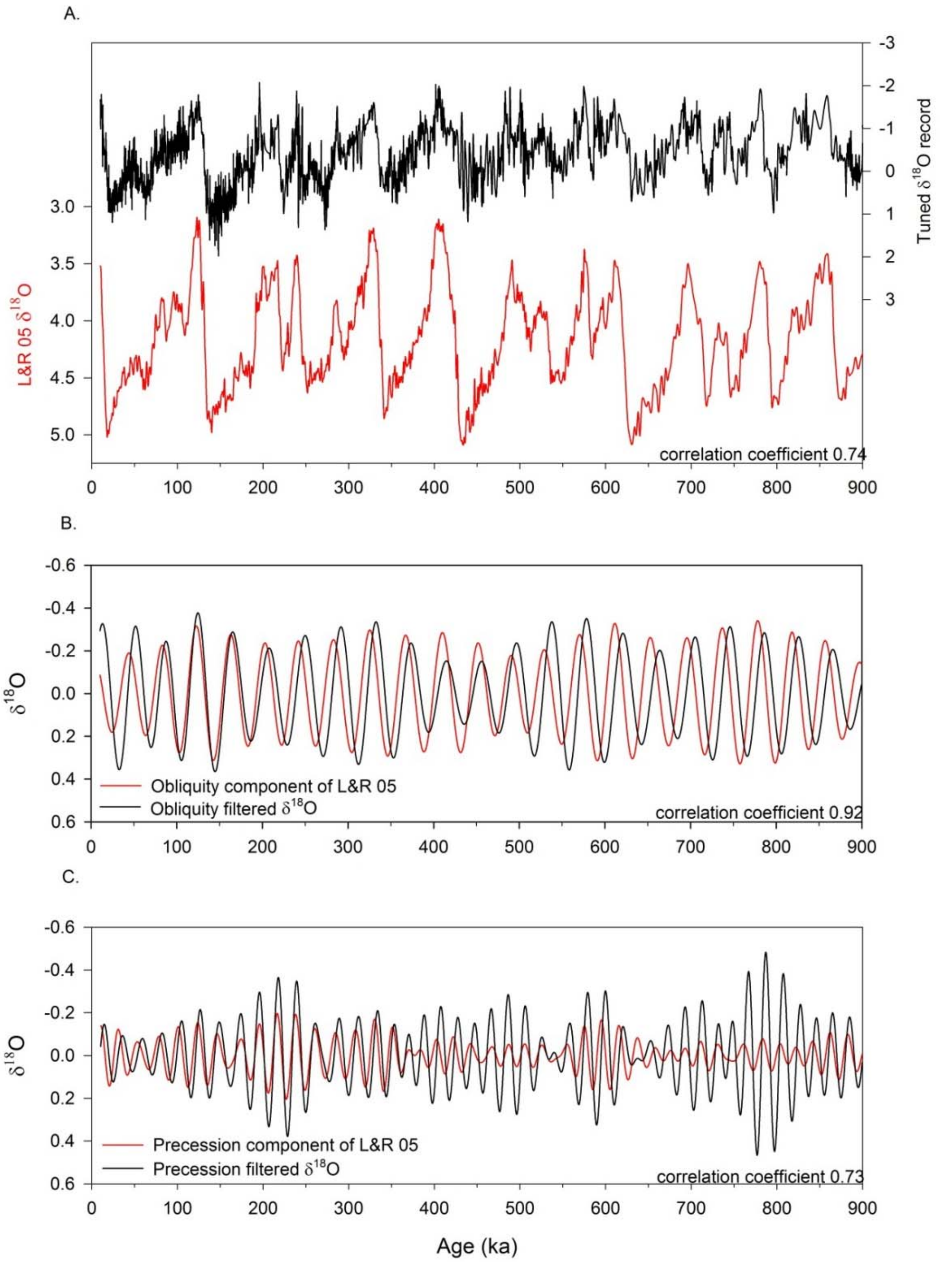

Figure B.21: (A) Comparison of the two records with a correlation coefficient of 0.74. (B) Both records filtered to remove frequencies lower than obliquity. Amplitude of the records fit well but the signals are consistently out of phase (C) Records filtered to display fit in precession components of the records. Overall, the filtered $\delta^{18}O$ signal has higher amplitude than the L&R 05 record.

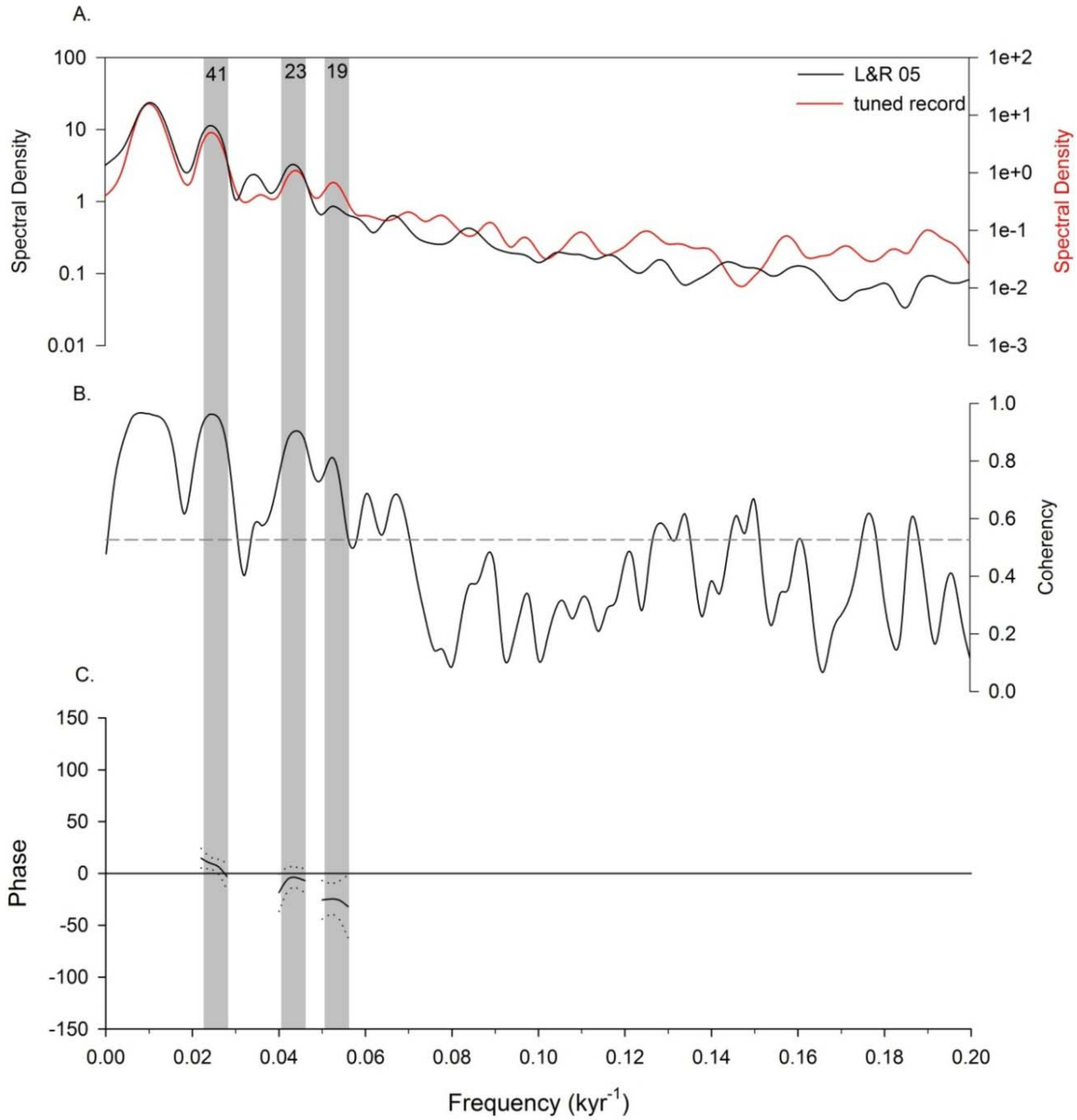

Figure B.22: (A) Cross spectral analysis of the Lisiecki and Raymo (2005) tuned $\delta^{18}O$ record. Spectral peaks occur at 41, 23, and 19 kyr periodicities (B) All three peaks have high coherence between the two records. (C) Plotted phase (black) and error bars (dotted line) indicates alignment of peaks between both time series. The obliquity peaks are out of phase by 797 years. The 23 and 19 kyr peaks are out of phase by 575 years and 1.4 kyr, respectively. The 23 kyr peak can be considered in phase based on the error bars.

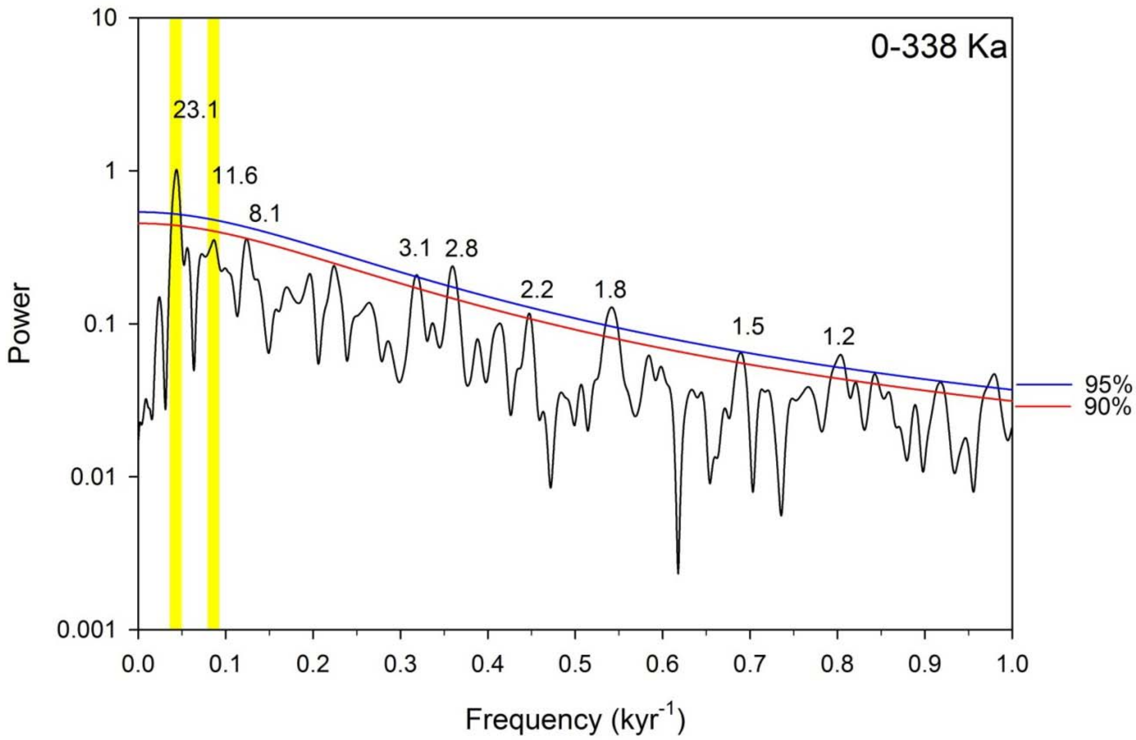

Figure B.23: Spectral analysis of the spliced $\delta^{18}O$ record in the subtropical northwestern Atlantic from 0-338 Ka tuned to Lisiecki and Raymo (2005). The record was high-pass filtered with a 247 year time step to remove periods longer than 33 kyr. The suborbital periodicity at 11.6 kyr has minor strength above an 80% CI and may be related to the 23.1 precessional peak but is not significant enough to be considered. There are no quarter precession signals present in the power spectrum and the 1.5 kyr signal is apparent. The persistence of the 1.5 kyr signal between age models indicates that the signal is robust and not artificial.

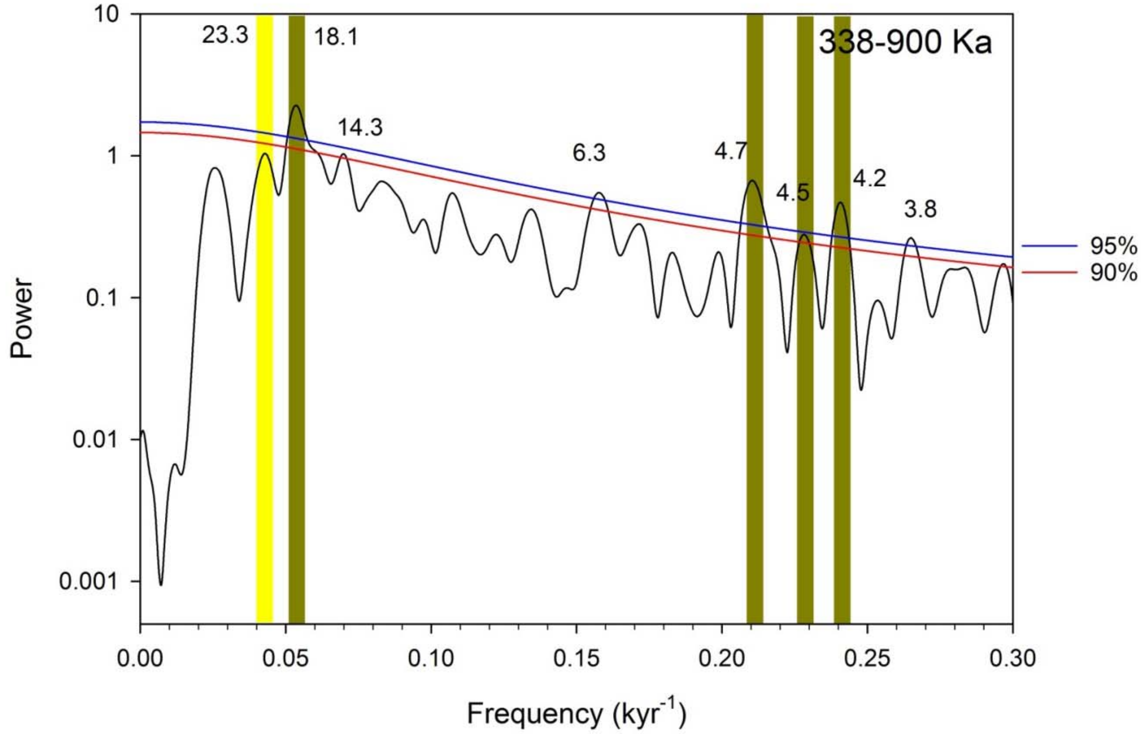

Figure B.24: Spectral analysis of the spliced and 33 kyr high band pass filtered $\delta^{18}O$ record from 338-875 Ka tuned to the Lisiecki and Raymo (2005) benthic $\delta^{18}O$ stack. There is a minor signal at 23.3 kyr periodicity barely above the 80% CI and a strong 18.1 kyr signal which are signals of precessional periodicity. No half precession cycle is observed. Peaks at 4.7, 4.5, and 4.2 kyr are within bandwidth of the 18.1 kyr peak and may be the quarter precession. The time step is 779 years, and higher frequency cycles are unresolved.

Appendix C

LEG 172 SITE 1059 OXYGEN ISOTOPE DATA

mcd	$\delta^{18}O$	Grützner Age Model (kyr)	1st Insolation Age Model (kyr)	2nd Insolation Age Model (kyr)	L&R Age Model (kyr)
39.12	-1.17	128.8			
39.17	-0.98	129.0			
39.22	-0.58	129.2			
39.27	-0.95	129.4			
39.32	-1.21	129.7			
39.37	-1.00	129.9			
39.42	-0.38	130.1			
39.47	-0.50	130.3			
39.52	-0.43	130.6			
39.57	-0.83	130.8	129.0	131.3	130.5
39.62	-0.73	131.0	129.2	131.6	130.9
39.67	-0.32	131.2	129.5	132.0	131.2
39.72	0.06	131.5	129.7	132.4	131.6
39.77	0.06	131.7	129.9	132.7	131.9
39.82	0.01	131.9	130.1	133.1	132.3
39.87	0.33	132.1	130.4	133.5	132.7
39.92	0.09	132.4	130.6	133.9	133.0
39.97	0.48	132.6	130.8	134.3	133.4
40.02	0.89	132.8	131.1	134.6	133.7
40.07	0.92	133.0	131.3	135.0	134.1
40.12	0.48	133.3	131.5	135.4	134.5
40.17	0.48	133.5	131.7	135.7	134.8
40.22	-0.04	133.7	132.0	136.1	135.2
40.27	0.73	134.0	132.2	136.5	135.5
40.32	0.63	134.2	132.4	136.9	135.9
40.37	0.83	134.4	132.6	137.3	136.3
40.42	0.98	134.6	132.9	137.6	136.6
40.47	1.05	134.9	133.1	138.0	137.0
40.52	1.27	135.1	133.3	138.1	137.2
40.57	1.02	135.3	133.5	138.1	137.4
40.62	0.88	135.5	133.7	138.1	137.5
40.67	0.84	135.6	133.8	138.2	137.6

40.72	1.18	135.7	133.9	138.2	137.7
40.77	1.60	135.8	134.1	138.2	137.8
40.82	0.76	136.0	134.2	138.2	137.9
40.87	0.10	136.1	134.3	138.3	138.0
40.92	0.60	136.2	134.4	138.3	138.1
40.97	0.96	136.3	134.6	138.3	138.2
41.02	0.86	136.5	134.7	138.4	138.3
41.07	0.63	136.6	134.8	138.4	138.4
41.12	0.76	136.7	134.9	138.4	138.5
41.17	0.87	136.8	135.0	138.4	138.6
41.22	0.98	136.9	135.2	138.5	138.7
41.27	1.12	137.1	135.3	138.5	138.8
41.32	0.91	137.2	135.4	138.5	138.9
41.37	0.85	137.3	135.5	138.6	139.0
41.42	0.89	137.4	135.7	138.6	139.1
41.47	0.94	137.6	135.8	138.6	139.2
41.52	0.80	137.7	135.9	138.6	139.4
41.57	0.98	137.8	136.0	138.7	139.5
41.62	1.10	137.9	136.2	138.7	139.6
41.67	1.27	138.0	136.3	138.7	139.7
41.72	1.22	138.2	136.4	138.7	139.8
41.77	1.30	138.3	136.5	138.8	139.9
41.82	0.73	138.4	136.6	138.8	140.0
41.87	1.06	138.5	136.8	138.8	140.1
41.92	1.22	138.7	136.9	138.9	140.2
41.97	1.18	138.8	137.0	139.0	140.3
42.02	0.85	138.9	137.1	139.1	140.4
42.07	0.85	139.0	137.3	139.1	140.5
42.12	0.83	139.1	137.4	139.2	140.6
42.17	1.05	139.3	137.5	139.3	140.7
42.22	0.95	139.4	137.6	139.4	140.8
42.27	0.78	139.5	137.7	139.4	140.9
42.32	0.71	139.6	137.9	139.5	141.0
42.37	0.69	139.8	138.0	139.6	141.1
42.42	1.03	139.9	138.1	139.7	141.2
42.47	0.92	140.0	138.2	139.7	141.3
42.52	0.99	140.1	138.4	139.8	141.4
42.57	0.86	140.2	138.5	139.9	141.5
42.62	1.02	140.4	138.6	140.0	141.6
42.67	0.96	140.5	138.7	140.0	141.7
42.72	0.89	140.6	138.8	140.1	141.8
42.77	0.94	140.7	139.0	140.2	141.9

42.82	1.18	140.9	139.1	140.3	142.1
42.87	0.80	141.0	139.2	140.3	142.2
42.92	0.86	141.1	139.3	140.4	142.3
42.97	1.19	141.2	139.5	140.5	142.4
43.02	1.11	141.3	139.6	140.6	142.5
43.07	0.93	141.5	139.7	140.6	142.6
43.12	0.77	141.6	139.8	140.7	142.7
43.17	0.79	141.7	139.9	140.8	142.8
43.22	0.89	141.8	140.1	140.9	142.9
43.27	0.89	142.0	140.2	140.9	143.0
43.32	0.89	142.1	140.3	141.0	143.1
43.37	0.92	142.2	140.4	141.1	143.2
43.42	0.55	142.3	140.6	141.1	143.2
43.36	1.02	142.2	140.4	141.1	143.3
43.41	1.44	142.3	140.5	141.1	143.3
43.46	0.83	142.4	140.7	141.2	143.4
43.51	0.86	142.5	140.8	141.3	143.5
43.56	1.36	142.7	140.9	141.4	143.6
43.61	1.43	142.8	141.0	141.4	143.7
43.66	1.69	142.9	141.1	141.5	143.8
43.71	0.57	143.0	141.3	141.6	143.9
43.76		143.2	141.4		
43.81	0.84	143.3	141.5	141.7	144.1
43.86	0.38	143.4	141.6	141.8	144.2
43.91	1.00	143.5	141.8	141.9	144.3
43.96	0.66	143.6	141.9	142.0	144.4
44.01	1.04	143.8	142.0	142.0	144.5
44.06	0.28	143.9	142.1	142.1	144.6
44.11	0.46	144.0	142.2	142.1	144.7
44.16	0.43	144.1	142.4	142.1	144.8
44.21	0.49	144.3	142.5	142.2	144.9
44.26	0.93	144.4	142.6	142.2	145.0
44.31	0.98	144.5	142.7	142.2	145.1
44.36	0.97	144.6	142.9	142.2	145.2
44.41	0.59	144.8	143.0	142.3	145.4
44.46	1.44	144.9	143.1	142.3	145.5
44.51	1.44	145.1	143.3	142.3	145.6
44.56	0.63	145.2	143.4	142.3	145.7
44.61	1.07	145.4	143.6	142.4	145.9
44.66	1.09	145.5	143.7	142.4	146.0
44.71	0.82	145.6	143.9	142.4	146.1
44.76	0.38	145.8	144.0	142.4	146.2

44.81	0.59	145.9	144.2	142.5	146.3
44.86	0.88	146.1	144.3	142.5	146.5
44.91	0.64	146.2	144.5	142.5	146.6
44.96	0.85	146.4	144.6	142.5	146.7
45.01	1.06	146.5	144.7	142.6	146.8
45.06	0.74	146.7	144.9	142.6	147.0
45.11	0.54	146.8	145.0	142.6	147.1
45.16	0.63	146.9	145.2	142.6	147.2
45.21	0.53	147.1	145.3	142.7	147.3
45.26	1.82	147.2	145.5	142.7	147.4
45.31	0.88	147.4	145.6	142.7	147.4
45.36		147.5	145.8		
45.41	0.37	147.7	145.9	142.7	147.6
45.46	0.67	147.8	146.0	142.7	147.6
45.51	0.42	148.0	146.2	142.7	147.7
45.56	1.69	148.1	146.3	142.7	147.7
45.61	0.79	148.3	146.5	142.8	147.8
45.66	0.87	148.4	146.6	142.8	147.9
45.71	1.98	148.5	146.8	142.8	147.9
45.76	0.64	148.7	146.9	142.8	148.0
45.81	0.19	148.8	147.1	142.8	148.0
45.86	1.26	149.0	147.2	142.8	148.1
45.91	0.33	149.1	147.3	142.8	148.2
45.96	1.05	149.3	147.5	142.8	148.2
46.01	1.34	149.4	147.6	142.8	148.3
46.06	1.41	149.6	147.8	142.9	148.3
46.11	1.27	149.7	147.9	142.9	148.4
46.16	1.37	149.8	148.1	142.9	148.4
46.21	1.41	150.0	148.2	142.9	148.5
46.26	1.39	150.1	148.4	142.9	148.6
46.31	1.33	150.3	148.5	142.9	148.6
46.36	1.35	150.4	148.7	142.9	148.7
46.41	0.43	150.6	148.8	142.9	148.7
46.46	1.22	150.7	148.9	143.0	148.8
46.51	1.05	150.9	149.1	143.0	148.9
46.56	0.98	151.0	149.2	143.0	148.9
46.61	0.75	151.1	149.4	143.0	149.0
46.66	1.05	151.3	149.5	143.0	149.0
46.71	1.03	151.4	149.7	143.0	149.1
46.76	0.34	151.6	149.8	143.0	149.2
46.81	0.86	151.7	150.0	143.0	149.2
46.86	0.71	151.9	150.1	143.1	149.3

46.91	1.17	152.0	150.2	143.1	149.3
46.96	1.07	152.2	150.4	143.1	149.4
47.01	1.10	152.3	150.5	143.1	149.5
47.06	0.84	152.5	150.7	143.1	149.5
47.11	0.95	152.6	150.8	143.1	149.6
47.16	0.99	152.7	151.0	143.1	149.6
47.21	0.90	152.9	151.1	143.1	149.7
47.26	0.99	153.0	151.3	143.1	149.7
47.31	1.04	153.2	151.4	143.2	149.8
47.36	0.90	153.3	151.6	143.2	149.9
47.41	0.82	153.5	151.7	143.2	149.9
47.46	1.08	153.6	151.8	143.2	150.0
47.46	1.20	153.6	151.8	143.2	150.0
47.51	1.16	153.8	152.0	143.2	150.0
47.56	0.93	153.9	152.1	143.2	150.1
47.61	0.99	154.0	152.3	143.2	150.1
47.66	1.24	154.2	152.4	143.2	150.2
47.71	1.02	154.3	152.6	143.3	150.3
47.76	0.97	154.5	152.7	143.3	150.3
47.81	0.90	154.6	152.9	143.3	150.4
47.86	1.07	154.8	153.0	143.3	150.4
47.91	0.76	154.9	153.1	143.3	150.5
47.96	1.18	155.1	153.3	143.3	150.6
48.01	0.91	155.2	153.4	143.3	150.6
48.06	1.14	155.3	153.6	143.3	150.7
48.11	0.66	155.5	153.7	143.4	150.7
48.16	0.93	155.6	153.9	143.4	150.8
48.21	1.16	155.8	154.0	143.4	150.9
48.26	0.02	155.9	154.2	143.4	150.9
48.31	1.12	156.1	154.3	143.4	151.0
48.36	1.20	156.2	154.4	143.4	151.0
48.41	1.05	156.4	154.6	143.4	151.1
48.46	0.80	156.5	154.7	143.4	151.2
48.51	1.28	156.7	154.9	143.4	151.2
48.56	1.18	156.8	155.0	143.5	151.3
48.61	1.07	156.9	155.2	143.5	151.3
48.66	1.16	157.1	155.4	143.5	151.4
48.71	1.22	157.3	155.6	143.5	151.5
48.76	1.01	157.5	155.8	143.5	151.6
48.81	1.37	157.7	156.0	143.5	151.6
48.86	1.45	157.9	156.2	143.6	151.7
48.91	0.84	158.1	156.4	143.6	151.8

48.96	0.82	158.4	156.6	143.6	151.9
49.01	0.64	158.6	156.8	143.6	152.0
49.06	0.63	158.8	157.0	143.6	152.1
49.11	0.85	159.0	157.2	143.6	152.1
49.16	0.58	159.2	157.4	143.7	152.2
49.21	0.75	159.4	157.6	143.7	152.3
49.26	0.83	159.6	157.8	143.7	152.4
49.31	0.83	159.8	158.0	143.7	152.5
49.36	0.67	160.0	158.2	143.7	152.6
49.41	0.81	160.2	158.4	143.7	152.6
49.46	0.81	160.4	158.6	143.8	152.7
49.51	0.61	160.6	158.8	143.8	152.8
49.56	0.76	160.8	159.0	143.8	152.9
49.61	0.88	161.0	159.2	143.8	153.0
49.66	0.86	161.2	159.5	143.8	153.1
49.71	0.73	161.4	159.7	143.8	153.2
49.76	0.83	161.6	159.9	143.9	153.2
49.81	0.40	161.8	160.1	143.9	153.3
49.86	0.95	162.0	160.3	143.9	153.4
49.91	0.62	162.2	160.5	143.9	153.5
49.96	0.34	162.5	160.7	143.9	153.6
50.01	0.24	162.7	160.9	143.9	153.6
50.06	0.92	162.9	161.1	144.0	153.7
50.11	0.79	163.1	161.3	144.0	153.8
50.16	0.81	163.3	161.5	144.0	153.9
50.21	0.51	163.5	161.7	144.0	154.0
50.26	0.67	163.7	161.9	144.0	154.1
50.31	0.37	163.9	162.1	144.0	154.1
50.36	0.78	164.1	162.3	144.1	154.2
50.41	0.65	164.3	162.5	144.1	154.3
50.46	0.77	164.5	162.7	144.1	154.4
50.51	0.81	164.7	162.9	144.1	154.5
50.56	0.97	164.9	163.1	144.1	154.6
50.61	0.70	165.1	163.3	144.1	154.6
50.66	0.74	165.3	163.6	144.2	154.7
50.71	0.66	165.5	163.8	144.2	154.8
50.76	0.55	165.7	164.0	144.2	154.9
50.81	0.56	165.9	164.2	144.2	155.0
50.86	0.50	166.1	164.4	144.2	155.1
50.91	1.05	166.3	164.6	144.3	155.1
50.96	0.90	166.6	164.8	144.3	155.2
51.01	1.19	166.8	165.0	144.3	155.3

51.06	1.00	167.0	165.2	144.3	155.4
51.11	0.95	167.2	165.4	144.3	155.5
51.16	0.80	167.4	165.6	144.3	155.6
51.21	0.63	167.6	165.8	144.4	155.6
51.26	0.88	167.8	166.0	144.4	155.7
51.31	0.59	168.0	166.2	144.4	155.8
51.36	0.60	168.2	166.4	144.4	155.9
51.41	0.19	168.4	166.6	144.4	156.0
51.46	0.12	168.6	166.8	144.4	156.1
51.51	0.24	168.8	167.0	144.5	156.1
51.56	0.38	169.0	167.2	144.5	156.2
51.61	0.54	169.2	167.4	144.5	156.3
51.66	1.12	169.4	167.7	144.5	156.4
51.71	0.94	169.6	167.9	144.5	156.5
51.76	0.91	169.8	168.1	144.5	156.6
51.81	0.88	170.0	168.3	144.6	156.6
51.86	1.09	170.3	168.5	144.6	156.7
51.91	0.60	170.5	168.8	144.6	156.8
51.96	0.64	170.8	169.0	144.6	157.0
52.01	0.70	171.1	169.3	144.6	157.1
52.06	0.71	171.3	169.6	144.7	157.2
52.11	0.65	171.6	169.9	144.7	157.3
52.16	0.69	171.9	170.1	144.7	157.4
52.21	0.65	172.2	170.4	144.7	157.5
52.26	0.79	172.4	170.7	144.8	157.6
52.31	0.76	172.7	170.9	144.8	157.7
52.36	0.86	173.0	171.2	144.8	157.8
52.41	0.70	173.3	171.5	144.8	157.9
52.46	0.88	173.5	171.8	144.9	158.1
52.51	0.52	173.8	172.0	144.9	158.2
52.56	0.96	174.1	172.3	144.9	158.3
52.51	0.53	173.8	172.0	144.9	158.2
52.56	0.67	174.1	172.3	144.9	158.3
52.61	1.17	174.4	172.6	145.0	158.4
52.66	1.00	174.6	172.9	145.0	158.5
52.71	0.48	174.9	173.1	145.1	158.6
52.76	0.94	175.2	173.4	145.1	158.7
52.81	1.08	175.5	173.7	145.1	158.9
52.86	0.86	175.7	174.0	145.2	159.1
52.91	1.13	176.0	174.2	145.3	159.3
52.96	0.51	176.3	174.5	145.3	159.5
53.01	0.71	176.5	174.8	145.4	159.7

53.06	0.51	176.8	175.1	145.4	159.9
53.11	0.34	177.1	175.3	145.5	160.1
53.16	0.05	177.4	175.6	145.6	160.3
53.21	0.57	177.6	175.9	145.6	160.5
53.26	0.64	177.9	176.1	145.7	160.7
53.30	0.78	178.1	176.4	145.7	160.8
53.35	0.74	178.4	176.6	145.8	161.0
53.40	0.20	178.7	176.9	145.8	161.2
53.45	0.89	179.0	177.2	145.9	161.4
53.50	0.69	179.2	177.5	146.0	161.6
53.55	0.62	179.5	177.7	146.0	161.8
53.60	0.87	179.8	178.0	146.1	162.0
53.65	0.34	180.0	178.3	146.1	162.2
53.70	0.77	180.3	178.6	146.2	162.3
53.75	0.61	180.6	178.8	146.3	162.5
53.80	0.69	180.9	179.1	146.3	162.7
53.85	0.39	181.1	179.4	146.4	162.9
53.90	0.87	181.4	179.6	146.4	163.1
53.95	0.65	181.7	179.9	146.5	163.3
54.00	0.42	181.9	180.2	146.6	163.5
54.05	0.75	182.2	180.4	146.6	163.7
54.10	0.60	182.4	180.6	146.7	163.8
54.15	0.46	182.6	180.9	146.7	164.0
54.20	0.53	182.9	181.1	146.8	164.2
54.25	0.66	183.1	181.3	146.8	164.3
54.30	0.60	183.3	181.5	146.9	164.5
54.35	0.41	183.5	181.8	146.9	164.6
54.40	0.73	183.8	182.0	147.0	164.8
54.45	0.50	184.0	182.2	147.0	165.0
54.50	0.78	184.2	182.5	147.1	165.1
54.55	-0.41	184.5	182.7	147.1	165.3
54.60	0.86	184.7	182.9	147.2	165.4
54.65	0.55	184.9	183.2	147.2	165.6
54.70	0.67	185.2	183.4	147.3	165.8
54.75	0.30	185.4	183.6	147.3	165.9
54.80	0.25	185.6	183.8	147.4	166.1
54.85	0.78	185.8	184.1	147.4	166.3
54.90	0.16	186.1	184.3	147.5	166.4
54.95	0.70	186.3	184.5	147.5	166.6
55.00	0.52	186.5	184.8	147.6	166.7
55.05	0.59	186.8	185.0	147.6	166.9
55.10		187.0	185.2		

55.15	0.79	187.2	185.5	147.7	167.2
55.20	-0.07	187.5	185.7	147.8	167.4
55.25	0.68	187.7	185.9	147.8	167.6
55.30	0.53	187.9	186.2	147.9	167.7
55.35	0.60	188.2	186.4	147.9	167.9
55.40	0.70	188.4	186.6	148.0	168.0
55.45	0.28	188.6	186.8	148.0	168.2
55.50	0.21	188.8	187.1	148.1	168.4
55.55	0.78	189.1	187.3	148.1	168.5
55.60	0.19	189.3	187.5	148.2	168.7
55.65	0.07	189.5	187.8	148.2	168.9
55.70	-0.34	189.8	188.0	148.3	169.0
55.75	0.21	190.0	188.2	148.3	169.2
55.80	-0.32	190.2	188.5	148.4	169.3
55.85	-0.23	190.5	188.7	148.4	169.5
55.90	-0.46	190.7	188.9	148.5	169.7
55.95	-0.35	190.9	189.1	148.5	169.8
56.00	0.10	191.1	189.4	148.6	170.0
56.05	-0.18	191.4	189.6	148.6	170.2
56.10	-0.39	191.6	189.8	148.7	170.3
56.15	0.08	191.8	190.1	148.7	170.5
56.20	-0.12	192.1	190.3	148.8	170.6
56.25	0.01	192.3	190.5	148.8	170.8
56.30		192.6	190.8		
56.35	-0.11	192.9	191.1	148.9	171.2
56.40	-0.20	193.2	191.4	149.0	171.4
56.45	0.26	193.5	191.7	149.0	171.6
56.50	-0.28	193.7	192.0	149.1	171.8
56.55		194.0	192.2		
56.60	-0.41	194.3	192.5	149.2	172.2
56.65	-0.36	194.6	192.8	149.3	172.4
56.70	0.01	194.9	193.1	149.3	172.6
56.75	-0.20	195.2	193.4	149.4	172.8
56.80	0.15	195.4	193.7	149.4	173.0
56.85	-0.41	195.7	194.0	149.5	173.2
56.90	-0.15	196.0	194.2	149.6	173.6
56.95	-0.11	196.3	194.5	149.7	174.0
57.00	-0.15	196.6	194.8	149.8	174.3
57.05	-0.15	196.9	195.1	149.9	174.7
57.10	0.13	197.1	195.4	149.9	175.0
57.15	-0.07	197.4	195.7	150.0	175.4
57.20	0.23	197.7	195.9	150.1	175.8

57.25	0.44	198.0	196.2	150.2	176.1
57.30	0.03	198.3	196.5	150.3	176.5
57.35		198.6	196.8		
57.40	0.03	198.8	197.1	150.5	177.2
57.45		199.1	197.4		
57.50	-0.38	199.4	197.6	150.7	178.0
57.55	-0.09	199.7	197.9	150.8	178.3
57.60	-0.26	200.0	198.2	150.9	178.7
57.65	0.00	200.3	198.5	151.0	179.0
57.70	-0.22	200.6	198.8	151.1	179.4
57.75		200.8	199.1		
57.80		201.1	199.4		
57.85	-0.17	201.4	199.6	151.4	180.5
57.90		201.7	199.9		
57.95		202.0	200.2		
58.00	-0.04	202.3	200.5	151.7	181.6
58.05	-0.54	202.5	200.8	151.8	182.0
58.10	0.00	202.7	201.0	151.8	182.2
58.15	-0.85	202.9	201.1	151.9	182.4
58.20		203.1	201.3		
58.25	-0.14	203.3	201.5	152.0	182.9
58.30	0.69	203.4	201.7	152.3	183.1
58.35	0.57	203.6	201.8	152.6	183.3
58.40	0.13	203.8	202.0	153.0	183.5
58.45	0.24	203.9	202.2	153.3	183.7
58.50	0.23	204.1	202.3	153.6	184.0
58.55	-0.03	204.3	202.5	153.9	184.2
58.60	0.03	204.5	202.7	154.2	184.4
58.65	0.37	204.6	202.9	154.5	184.6
58.70	0.09	204.8	203.0	154.9	184.9
58.75		205.0	203.2		
58.80	-0.07	205.2	203.4	155.5	185.3
58.85		205.3	203.6		
58.90	-0.11	205.5	203.7	156.1	185.7
58.95	-0.57	205.7	203.9	156.4	186.0
59.00	0.02	205.8	204.1	156.8	186.2
59.05	0.10	206.0	204.2	157.1	186.4
59.10	-0.11	206.2	204.4	157.4	186.6
59.15	0.18	206.4	204.6	157.7	186.8
59.20	0.02	206.5	204.8	158.0	187.1
59.25	0.47	206.7	204.9	158.4	187.3
59.30	-0.74	206.9	205.1	158.8	187.5

59.35	0.22	207.0	205.3	159.2	187.7
59.40	0.24	207.2	205.4	159.5	187.9
59.45	-0.09	207.4	205.6	160.0	188.2
59.50	0.25	207.6	205.8	160.5	188.5
59.55	-0.03	207.7	206.0	160.9	188.7
59.60	0.28	207.9	206.1	161.4	189.0
59.65	-0.09	208.1	206.3	161.9	189.3
59.70	-0.26	208.3	206.5	162.4	189.6
59.65	-0.24	208.1	206.3	161.9	189.3
59.70	0.11	208.3	206.5	162.4	189.6
59.75	-0.04	208.4	206.7	162.9	189.9
59.80		208.6	206.8		
59.85	-0.18	208.8	207.0	163.9	190.4
59.90	-0.52	208.9	207.2	164.4	190.7
59.95	-1.30	209.1	207.3	164.8	191.0
60.00	-0.94	209.3	207.5	165.3	191.3
60.05	-0.94	209.5	207.7	165.8	191.6
60.10	-0.73	209.6	207.9	166.3	191.8
60.15	-0.93	209.8	208.0	166.8	192.1
60.20	-0.83	210.0	208.2	167.3	192.4
60.25	-0.37	210.1	208.4	167.8	192.7
60.30	-1.00	210.3	208.5	168.2	192.9
60.35	-0.70	210.5	208.7	168.7	193.2
60.40	-0.41	210.7	208.9	169.2	193.5
60.45	-0.44	210.8	209.1	169.7	193.8
60.50	-0.44	211.0	209.2	170.2	194.1
60.55	-0.77	211.2	209.4	170.7	194.3
60.60	-0.51	211.4	209.6	171.2	194.6
60.65	-0.84	211.5	209.8	171.7	194.9
60.70	-1.43	211.7	209.9	172.1	195.2
60.75	-1.56	211.9	210.1	172.6	195.5
60.80	-2.03	212.0	210.3	173.0	195.7
60.85	-1.83	212.2	210.4	173.3	196.0
60.90		212.4	210.6		
60.95		212.6	210.8		
61.00	-0.84	212.7	211.0	175.2	197.8
61.05	-0.52	212.9	211.1	175.8	198.3
61.10	-0.83	213.1	211.3	176.4	198.9
61.15	-0.01	213.2	211.5	177.0	199.5
61.20	-0.56	213.4	211.7	177.6	200.1
61.25	-0.65	213.6	211.8	178.2	200.6
61.30	-0.89	213.8	212.0	178.9	201.2

61.35	-0.58	214.1	212.3	180.0	202.3
61.40		214.5	212.7		
61.45		214.8	213.1		
61.50	-0.43	215.2	213.4	183.9	206.0
61.55		215.6	213.8		
61.60	-0.39	215.9	214.1	186.5	207.8
61.65	-0.39	216.3	214.5	187.9	208.6
61.70	-1.22	216.6	214.9	189.3	209.5
61.75	-0.59	217.0	215.2	190.7	210.3
61.80	-1.02	217.4	215.6	192.0	211.2
61.85		217.7	216.0		
61.90	-0.29	218.1	216.3	194.8	212.9
61.95	-0.91	218.5	216.7	195.7	213.7
62.00	-0.98	218.8	217.1	196.5	214.6
62.05		219.2	217.4		
62.10	-1.05	219.6	217.8	198.1	216.3
62.15	-1.27	219.9	218.2	199.0	217.2
62.20	-1.17	220.3	218.5	199.9	218.0
62.25	-0.27	220.7	218.9	200.7	218.9
62.30	-0.18	221.0	219.3	201.6	219.7
62.35	0.07	221.4	219.6	202.5	220.6
62.40	0.48	221.8	220.0	203.4	221.4
62.45		222.1	220.3		
62.50	0.20	222.5	220.7	205.1	223.1
62.55	0.98	222.8	221.1	206.0	224.0
62.60	0.55	223.2	221.4	207.1	225.3
62.65		223.6	221.8		
62.70	0.31	223.9	222.2	207.8	226.4
62.75	-0.29	224.3	222.5	208.2	226.9
62.80	-0.30	224.7	222.9	208.6	227.4
62.85	0.04	225.0	223.3	209.0	227.9
62.90	0.58	225.4	223.6	209.4	228.5
62.95	0.27	225.7	223.9	209.7	228.9
63.00	-0.06	226.0	224.2	210.0	229.3
63.05	0.16	226.3	224.5	210.3	229.7
63.10	-0.16	226.6	224.8	210.6	230.1
63.15	-0.38	226.9	225.1	210.9	230.5
63.20	-0.23	227.1	225.4	211.3	231.0
63.25	-0.44	227.4	225.7	211.6	231.4
63.30	0.21	227.7	226.0	211.9	231.8
63.35	0.18	228.0	226.2	212.2	232.2
63.40	0.22	228.3	226.5	212.5	232.6

63.45	-0.37	228.6	226.8	212.8	233.0
63.50	-0.08	228.9	227.1	213.1	233.4
63.55	-0.74	229.2	227.4	213.4	233.9
63.60	-0.97	229.5	227.7	213.7	234.3
63.65	-0.89	229.8	228.0	214.0	234.7
63.70	-0.19	230.1	228.3	214.4	235.1
63.75	-0.04	230.3	228.6	214.7	235.5
63.80	-0.70	230.6	228.9	215.0	235.9
63.85	-0.50	230.9	229.2	215.3	236.4
63.90	-0.98	231.2	229.5	215.6	236.8
63.95	-0.61	231.5	229.7	215.9	237.2
64.00	-0.27	231.8	230.0	216.2	237.6
64.05	-1.00	232.1	230.3	216.5	238.0
64.10	-1.22	232.4	230.6	216.8	238.4
64.15	-1.44	232.7	230.9	217.1	238.9
64.20	-1.87	233.0	231.2	217.4	239.3
64.25	-0.84	233.3	231.5	217.7	239.6
64.30	-0.65	233.6	231.8	217.8	239.7
64.24	-1.10	233.2	231.4	218.0	240.0
64.29	-0.77	233.5	231.7	218.1	240.1
64.34	-1.18	233.8	232.0	218.5	240.4
64.39	-0.65	234.1	232.3	219.0	240.8
64.44	1.30	234.4	232.6	219.6	241.3
64.49	-1.47	234.7	232.9	220.1	241.7
64.54	-0.42	234.9	233.2	220.6	242.1
64.59	-0.02	235.2	233.5	221.1	242.5
64.64	-0.82	235.5	233.8	221.6	242.9
64.69	0.61	235.8	234.1	222.1	243.3
64.74	0.22	236.1	234.3	222.6	243.8
64.79		236.4	234.6		
64.84	0.13	236.7	234.9	223.6	244.6
64.89	-0.32	237.0	235.2	224.2	245.0
64.94		237.3	235.5		
64.99	-1.49	237.6	235.8	225.2	245.8
65.04	0.49	237.8	236.1	225.7	246.2
65.09	0.59	238.1	236.3	226.1	246.6
65.14	0.47	238.3	236.5	226.5	246.9
65.19	0.42	238.6	236.8	226.9	247.2
65.24	0.08	238.8	237.0	227.4	247.6
65.29	0.24	239.0	237.3	227.8	247.9
65.34	0.22	239.3	237.5	228.2	248.2
65.39	0.58	239.5	237.7	228.6	248.6

65.44	0.20	239.7	238.0	229.0	248.9
65.49	0.18	240.0	238.2	229.4	249.3
65.54	0.67	240.2	238.4	229.8	249.6
65.59	0.37	240.4	238.7	230.2	249.9
65.64	0.42	240.7	238.9	231.0	250.5
65.69	0.07	240.9	239.1	232.7	251.2
65.74	0.50	241.1	239.4	234.3	251.8
65.79	0.32	241.4	239.6	236.0	252.4
65.84	-0.59	241.6	239.8	237.7	253.0
65.89	-0.14	241.8	240.1	239.4	253.7
65.94	0.13	242.1	240.3	241.0	254.3
65.99	-0.67	242.3	240.5	242.0	254.9
66.04	-0.07	242.5	240.8	242.9	255.5
66.09	-0.22	242.8	241.0	243.9	256.2
66.14	0.06	243.0	241.2	244.8	256.8
66.19	-0.04	243.2	241.5	245.8	257.4
66.24	-0.22	243.5	241.7	246.7	258.0
66.29	0.19	243.7	241.9	247.7	258.7
66.34	-0.29	244.0	242.2	248.6	259.3
66.39	0.45	244.2	242.4	249.6	259.9
66.44	0.17	244.4	242.7	250.5	260.5
66.49	-0.24	244.7	242.9	251.5	261.2
66.54	0.19	244.9	243.1	252.4	261.8
66.59	-0.03	245.1	243.4	253.4	262.4
66.64	-0.15	245.4	243.6	254.3	263.0
66.69	0.51	245.6	243.8	255.3	263.6
66.74	0.27	245.8	244.1	256.3	264.3
66.79	0.22	246.1	244.3	257.2	264.9
66.84	-0.02	246.3	244.5	258.2	265.5
66.89	0.52	246.5	244.8	259.1	266.1
66.94	0.46	246.8	245.0	260.1	266.7
66.99	0.16	247.0	245.2	261.0	267.4
67.04	-0.72	247.2	245.5	261.6	268.0
67.09	0.29	247.5	245.7	262.2	268.2
67.14	0.27	247.7	245.9	262.8	268.4
67.19	0.30	247.9	246.2	263.4	268.5
67.24	0.57	248.2	246.4	264.0	268.7
67.29	0.68	248.4	246.6	264.6	268.9
67.34		248.6	246.9		
67.39	0.38	248.9	247.1	265.8	269.2
67.44	0.38	249.1	247.3	266.4	269.4
67.49	0.43	249.4	247.6	267.0	269.6

67.54	0.38	249.6	247.8	267.6	269.8
67.59	0.49	249.8	248.0	268.2	269.9
67.64	0.55	250.1	248.3	268.8	270.1
67.69	0.36	250.3	248.5	269.4	270.3
67.74	0.41	250.5	248.8	270.0	270.5
67.79	0.64	250.8	249.0	270.6	270.6
67.84	0.69	251.0	249.2	271.2	270.8
67.89	0.67	251.2	249.5	271.8	271.0
67.94	0.91	251.5	249.7	272.4	271.6
67.99	1.17	251.7	249.9	272.5	271.7
68.04	0.84	251.9	250.2	272.6	271.8
68.09	0.65	252.2	250.4	272.7	271.8
68.14	0.32	252.4	250.6	272.7	271.9
68.19	0.71	252.6	250.9	272.8	272.0
68.24	0.33	252.9	251.1	272.9	272.1
68.29	0.69	253.1	251.3	273.0	272.2
68.34	1.33	253.3	251.6	273.1	272.3
68.39	-0.09	253.6	251.8	273.2	272.4
68.44		253.8	252.0		
68.49	0.58	254.0	252.3	273.4	272.6
68.54	0.05	254.3	252.5	273.5	272.6
68.59		254.5	252.7		
68.64	0.53	254.7	253.0	273.6	272.8
68.69	0.51	255.0	253.2	273.7	272.9
68.74	0.62	255.2	253.4	273.8	273.0
68.79	0.89	255.5	253.7	273.9	273.1
68.84	0.47	255.7	253.9	274.0	273.2
68.89	0.47	255.9	254.2	274.1	273.3
68.94	0.81	256.2	254.4	274.2	273.4
68.99	0.75	256.4	254.6	274.3	273.4
69.04	0.23	256.6	254.9	274.4	273.5
69.09	0.39	256.9	255.1	274.5	273.6
69.14	0.82	257.1	255.3	274.5	273.7
69.19	0.77	257.3	255.6	274.6	273.8
69.24		257.6	255.8		
69.29	0.39	257.8	256.0	274.8	274.0
69.34	1.26	258.0	256.3	274.9	274.1
69.39		258.3	256.5		
69.44	1.00	258.5	256.7	275.1	274.2
69.49	0.93	258.8	257.0	275.2	274.3
69.54	0.74	259.0	257.2	275.3	274.4
69.59	0.54	259.3	257.5	275.4	274.5

69.64		259.5	257.8		
69.69	0.65	259.8	258.0	275.6	274.7
69.74	0.45	260.0	258.3	275.7	274.8
69.79	0.11	260.3	258.5	275.8	274.9
69.84	0.57	260.6	258.8	275.9	275.0
69.89	0.48	260.8	259.0	276.1	275.1
69.94	0.12	261.1	259.3	276.2	275.2
69.99		261.3	259.6		
70.04	0.18	261.6	259.8	276.4	275.4
70.09	0.41	261.8	260.1	276.5	275.5
70.14	0.50	262.1	260.3	276.6	275.6
70.19	0.64	262.3	260.6	276.7	275.7
70.24	0.60	262.6	260.8	276.8	275.8
70.29		262.9	261.1		
70.34	0.84	263.1	261.3	277.0	276.0
70.39		263.4	261.6		
70.44	0.17	263.6	261.9	277.2	276.2
70.49	-0.13	263.9	262.1	277.3	276.3
70.54	0.26	264.1			
70.59	0.21	264.4			
70.64	-0.02	264.7			
70.69	0.42	264.9			
70.74	0.32	265.2			
70.79	0.01	265.4			
70.84	0.30	265.7			
70.89	0.19	265.9			
70.94	0.46	266.2			
70.99	0.22	266.5			
71.04	0.51	266.7			
71.09	0.14	267.0			
71.14	-0.08	267.2			